WADD TECHNICAL REPORT 60-699
VOLUME I

ENERGY CONVERSION SYSTEMS REFERENCE HANDBOOK

VOLUME I — GENERAL SYSTEM CONSIDERATIONS

W. R. Menetrey
J. H. Fisher

Electro-Optical Systems, Inc.

SEPTEMBER 1960

Flight Accessories Laboratory
Contract Nr. AF 33(616)-6791
Project Nr. 4769
Task Nr. 61048

WRIGHT AIR DEVELOPMENT DIVISION
AIR RESEARCH AND DEVELOPMENT COMMAND
UNITED STATES AIR FORCE
WRIGHT-PATTERSON AIR FORCE BASE, OHIO

700 — May 1961 — 30-1125

FOREWORD

This report entitled "Energy Conversion Systems Reference Handbook," was prepared by Electro-Optical Systems, Inc., under Air Force Contract AF 33(616)-6791, Project Nr 4769, and Task Nr 61048. The work was administered under the direction of the Flight Accessories Laboratory, Wright Air Development Division. Acknowledgment is made for the assistance provided by personnel of the Flight Vehicle Power Branch of the Flight Accessories Laboratory.

The studies presented began in September 1959 and were concluded in August 1960. They represent the joint efforts of members of the staff of Electro-Optical Systems, Inc. directed by W. R. Menetrey, Project Supervisor.

The cooperation of Atomics International, The Martin Company, Massachusetts Institute of Technology, and AiResearch Manufacturing Company is gratefully acknowledged.

This report concludes the work under contract AF33(616)-6791.

A B S T R A C T

Volume I serves as an introduction to subsequent volumes dealing with specific areas of power system technology. General topics useful in evaluating and rating power systems are discussed including the space environment and its effects; reliability considerations in systems design; figures of merit and their use in system evaluation; power needs of the future and the importance of developing power systems; and an estimate of expected system weights. Environmental effects include meteoroid bombardment, interplanetary and Van Allen Corpuscular Radiation, electromagnetic solar radiation, and vacuum. It is shown that the effort needed to guarantee high power system reliability may be too costly. The relative position of nuclear, chemical, and solar power systems in a power level-mission duration continuum is presented.

ENERGY CONVERSION SYSTEMS REFERENCE HANDBOOK

LIST OF VOLUME AND SECTION TITLES WITH AUTHORS

ENERGY CONVERSION SYSTEMS REFERENCE HANDBOOK

LIST OF VOLUME AND SECTION TITLES WITH AUTHORS (CONT'D)

A complete detailed Table of Contents for all volumes of Energy Conversion Systems Reference Handbook is included in Volume I.

ENERGY CONVERSION SYSTEMS REFERENCE HANDBOOK

TABLE OF CONTENTS

TABLE OF CONTENTS (CONTINUED)

TABLE OF CONTENTS (CONTINUED)

TABLE OF CONTENTS (CONTINUED)

ENERGY CONVERSION SYSTEMS REFERENCE HANDBOOK

TABLE OF CONTENTS (CONTINUED)

TABLE OF CONTENTS (CONTINUED)

TABLE OF CONTENTS (CONTINUED)

TABLE OF CONTENTS (CONTINUED)

ENERGY CONVERSION SYSTEMS REFERENCE HANDBOOK

TABLE OF CONTENTS (CONTINUED)

ENERGY CONVERSION SYSTEMS REFERENCE HANDBOOK

TABLE OF CONTENTS (CONTINUED)

TABLE OF CONTENTS (CONTINUED)

TABLE OF CONTENTS (CONTINUED)

TABLE OF CONTENTS (CONTINUED)

TABLE OF CONTENTS (CONTINUED)

TABLE OF CONTENTS (CONTINUED)

TABLE OF CONTENTS (CONTINUED)

TABLE OF CONTENTS (CONTINUED)

TABLE OF CONTENTS (CONTINUED)

TABLE OF CONTENTS (CONTINUED)

TABLE OF CONTENTS (CONTINUED)

TABLE OF CONTENTS (CONTINUED)

TABLE OF CONTENTS (CONTINUED)

TABLE OF CONTENTS (CONTINUED)

ENERGY CONVERSION SYSTEMS REFERENCE HANDBOOK

Volume I - General System Considerations

Section A

INTRODUCTION

W. R. Menetrey
Energy Research Division
ELECTRO-OPTICAL SYSTEMS, INC.

Manuscript released by the author
September 1960 for publication in this
Energy Conversion Systems Reference Handbook

I-A INTRODUCTION

C O N T E N T S
and
I L L U S T R A T I O N S

I-A INTRODUCTION

This final report entitled "Energy Conversion Systems Reference Handbook", summarizes the studies and analysis accomplished under Contract AF 33(616)-6791, extending from 1 September 1959 to 31 August 1960. The primary objective of this study was a thorough evaluation of power sources and energy converters which are space applicable and are being used, built or being developed.

A tremendous number of devices and physical phenomena appear useful in space power systems, as indicated by a perusal of the table of contents. A wide variety of systems -- chemical, solar, and nuclear -- will be required to satisfy the complexity and scope of future planned missions. It appears impossible at this time to eliminate any of the major types of power systems under consideration as each will find a niche in the power level - mission duration continuum where it appears most useful. Each of the major types of dynamic and static converters discussed in this handbook merit further investigation.

The projection of system performance is particularly difficult due to the lack of experience in solving a large number of practical problems remaining before many new systems can be launched into space. Estimates of reliability and the effects of the space environment are in many cases little more than conjecture due to the lack of concrete test data. Weight is a figure of merit popularly used to compare systems. However, a realistic weight estimate must be related to a specific system and such items as alteration of the missile necessary to contain and use the power system, cooling requirements imposed on the rest of the vehicle, and other factors not usually included in a preliminary weight analysis.

System cost is also misleading as a basis for selection unless other items such as launch cost are included.

Another difficulty in evaluating systems lies in the fact that the usefulness of energy conversion phenomena is dependent on new, constantly changing material parameters and device fabrication techniques. This is a direct consequence of the almost exponential characteristic growth of research and development. The projection of system performance, consequently, always contains a degree of uncertainty.

Keeping in mind these limitations, the results presented here establish the types of missions where a specific system might be useful, the approximate weights of these systems, empirical and analytical relations describing their performance, changes in performance anticipated in the future, and other characteristics of interest.

The importance of a document of this type is apparent from the tremendous increase in attention and funding received in this technical area in the last few years. The Air Force for example, has increased research funding in this area sixteen-fold in the past three years. The term "secondary" or "auxiliary" power is now a misnomer. It has, in general, been dropped from government terminology, using instead terms such as "flight vehicle power."

For the purposes of systematizing the assignment of manpower facilities and money to expedite research, the ARDC has subdivided flight vehicle power into six segments. These segments are delineated in Figure I-A-1 along with the projected effects of research on future vehicles, as evaluated in a WADD planning model for flight vehicle power*. As shown, research in flight vehicle

*Shows, H. R. "The 'Not So Auxiliary' Power Systems," Aircraft and Missiles, July 1960.

WORK SEGMENTS	BALLISTIC MISSILES	AERODYNAMIC MISSILES	AIRCRAFT	BOOST GLIDE	SATELLITES	LUNAR FLIGHT	PLANETARY
ENERGY SOURCES	0	3	3	3	7	8	8
ENERGY CONVERSION STATIC	0	2	1	3	8	8	8
ENERGY CONVERSION DYNAMIC	3	6	5	7	6	6	7
FLUID TRANS.	3	7	7	8	5	7	6
ELECT. TRANS.	3	6	7	7	7	7	7
SYSTEM ANALYSIS	1	3	3	5	7	8	8

(Vehicle Types)

Numerical Rating	Definition of Rating
9	Essential to attainment of design mission capability and will permit revolutionary improvement of performance beyond the design mission capability.
7	Essential to attainment of design mission capability and would provide adequate performance for the design mission capability.
5	Essential contribution toward attainment of design capability but would provide performance significantly less than desired for the design mission capability.
3	Not essential to attainment of design mission capability but would permit small improvement beyond design mission capability.
2	Not essential to attainment of design mission capability but would provide economy and/or convenience to the design mission capability.
0	Negligible improvement.

FIGURE I-A-1 EFFECT OF FLIGHT VEHICLE POWER ON FUTURE VEHICLES

power is essential if adequate performance is to be attained with future space vehicle designs.

A wide variety of power systems and components will be available in the near future to satisfy power demands. This report is primarily concerned with the following areas (see Figure I-A-1): energy sources, static energy converters, dynamic energy converters, system analysis, and electrical transmission to some extent.

1.0 PROGRAM OBJECTIVES AND REQUIREMENTS

The primary objectives of this study were:

a. To evaluate power sources and energy converters which are applicable to space and are being used, built or being developed.

b. To present the technical information resulting from this program in a usable form which serves as a guide in energy research programs for national defense.

The analysis is bounded by the following conditions regarding missions and systems of interest:

a. Electrical power is the desired form of energy output and various hydraulic, pneumatic or mechanical transmission systems are not considered.

b. Anticipated performance is projected 10 years into the future. Consequently, analysis includes promising theoretical developments as well as current experimental components. The period beyond 10 years is not extensively explored.

c. System power levels lie roughly between 10 watt and 20 mw and a constant electrical load is desired.

d. Load durations are greater than one hour. However, some consideration is given to storage systems which can be applied for short term peak load application.

These studies are directed towards satellites, lunar flight, planetary and related vehicles. The satellite has been assumed to have a circular orbit. A large number of manned and unmanned Earth, lunar, Mars, Venus and other miscellaneous probes are likely to be attempted within the next decade. The choice of power system and the amount of energy required will depend on a large number of factors determined by the mission including:

a. Objectives - e.g., scientific exploration, military operations, commercial operations.

b. Instrument or manned operation.

c. Type of mission as it affects the incidence of solar radiation and the need for energy storage - space flight continuously in sun, satellite requiring energy storage, surface operations which may require period of shadow operation, surface propulsion power, permanent manned base.

d. Propulsion or secondary electrical power system.

e. Payload weight and volume limitations.

f. Future state-of-the-art.

g. Cost.

In general the power required will consist of a series of peak, short duration drains superimposed on a lower average continuous load. Average power requirements are difficult to estimate due to the variety of mission requirements. Figure I-A-2 displays probable space power requirements as estimated

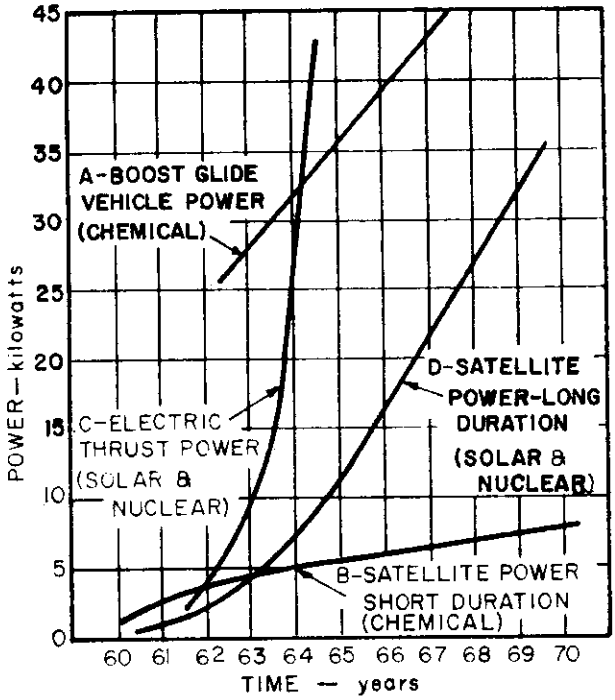

FIGURE I-A-2 ESTIMATED SPACE POWER REQUIREMENTS

by Jones and Keeler*. These estimates roughly concur within a factor of two with other published figures. As shown, long duration power requirements are about 2.5 kw in 1962, 12 kw in 1965, and 37 kw in 1970. Megawatts of power will be required for interplanetary electrical propulsion and for permanent manned bases on the moon and planets.

2.0 HANDBOOK ORGANIZATION

The organization of this handbook is indicated by the Table of Contents. It consists of 11 volumes. The first volume serves as an introduction and discusses general topics useful in system selection.

Volumes II through VIII are concerned with specific system components which may be combined in a variety of ways. The type of information provided in these volumes includes:

a. The basic physical model which describes the physical phenomena taking place in the energy converter and the classification of device types.

b. The theoretical and empirical relations which govern the design of the component, and their validity.

c. The sources of energy loss in the practical converter and avenues of approach towards decreasing loss.

d. Parametric studies showing the effect of design variations and the optimization of parameters.

e. Current experimental and fabrication programs and the results of these programs.

*Jones, R. A. and Keeler, J.S., "Flight Vehicle Power". SAE Paper 105U, SAE National Aero Meeting, October 5-9, 1959.

f. Present and anticipated design and performance characteristics.

Volumes IX through XI use this information to derive trends in power system cost, weight, and reliability.

Volume IX describes the performance characteristics of solar power systems, using both photovoltaic cells and thermal converters. Volume XI describes radioisotope power systems under development and being planned. Shielding, safety, reliability, and related subjects are discussed in detail. Weight, cost and other performance characteristics are given for radioisotope systems employing static and dynamic converters. Volume XI was prepared by The Martin Company and was made available to Electro-Optical Systems, Inc., by arrangement with the AEC for inclusion in this handbook.

Volume X presents a detailed description of the nuclear space power systems presently under development. In addition, weight and performance estimates are given for higher power and more advanced nuclear systems employing thermoelectric, turboelectric and thermionic power conversion methods. Various aspects of reactor design are discussed with respect to inherent limitations and system requirements. Many problems which are common to all nuclear systems such as shielding, reliability, heat rejection, safety, and operational considerations are presented in some detail.

Volume X was prepared by Atomics International, a Division of North American Aviation under contract to the Missiles Project Branch of the Atomic Energy Commission. Volume X, **classified Secret Restricted Data,** can be obtained with proper clearance from the AEC -- Document No. NAA-SR-5650.

3.0 OBTAINING INFORMATION

Information was obtained through literature surveys and personal interview. Literature sources included ASTIA, government agency and private company reports, patent files, open technical literature and other sources.

Electro-Optical Systems, Inc., has previously conducted programs of a similar nature. This information was repeated only where necessary for reporting continuity. References to this work can be obtained in the following documents:

> Memorandum No. 20-164, Jet Propulsion Laboratory, Pasadena, "A Study of Energy Sources"
>
> WADC Technical Report No. 59-17 "Analysis of Solar Energy Utilization"

It should be noted that excellent surveys regarding several specific components are already available in the open literature. These surveys are referenced. In addition, literature bibliographies are available from several government organizations which materially aid in the tracing of pertinent material. Also, several organizations have conducted programs similar in nature to this contract (AF 33(616)-6791), with brief analyses which have determined the comparative weights of various systems. These results were incorporated where applicable.

A great deal of information was gained by interviewing personnel in government and private laboratories. Inquiries were made into the theoretical and practical aspects of component subsystem and system design and fabrication. It was emphasized that this final report would be read by industrial and government personnel. Consequently no information contained in this report can be considered proprietary.

Large national technical society meetings tend to draw together a great number of people and can be used not only to gain specific information concerning the papers given but also for profitable discussion with audience members and speakers. The programs for these meetings and papers of significant interest were acquired, and several were attended.

4.0 ACKNOWLEDGEMENTS

A major portion of the text was prepared by the members of the technical staff of Electro-Optical Systems, Inc. The author of each individual section is properly accredited in each case. Several companies volunteered to undertake the task of summarizing specific areas of technology in which they were acknowledged leaders. These include:

Atomics International	-	Reactor System Design, Vol. X;
Martin Aircraft Company	-	Radioisotopes System Design, Vol. XI.

In addition, two sections were written under subcontract:

1. AiResearch Manufacturing Company - Non-Phase-Change Heat Exchangers, Volume VII, Section B.
2. John Blair, Assoc. (M.I.T.) - Thermoelectric Generators, Volume IV, Section A.

I-B SPACE ENVIRONMENTAL CONDITIONS

C O N T E N T S

ENERGY CONVERSION SYSTEMS REFERENCE HANDBOOK

Volume I - General System Considerations

Section B

SPACE ENVIRONMENTAL CONDITIONS

W. R. Menetrey
Energy Research Division
ELECTRO-OPTICAL SYSTEMS, INC.

Manuscript released by the author
September 1960 for publication in this
Energy Conversion Systems Reference Handbook

I-B SPACE ENVIRONMENTAL CONDITIONS

ILLUSTRATIONS and TABLES

I-B SPACE ENVIRONMENTAL CONDITIONS

The design of any power system will be strongly affected by the environmental conditions encountered in space operation. The system will, of course, necessarily be designed to withstand conditions of vibration, shock, acceleration, temperature rise and other factors encountered during launch. Space environmental conditions of importance will include:

a. Vacuum - Experiment has shown that most materials of inorganic nature will experience negligible mass loss during long periods in a vacuum environment. Certain materials and alloys of these materials must be avoided, however, including alkali metals, magnesium and zinc. Aluminum exhibits negligible evaporation at the anticipated temperature of operation.

The selection of plastics which will maintain structural integrity in a vacuum is limited but several with useful characteristics in space are available if material temperatures of less than roughly 200^{o}F can be maintained.

The performance of bearings exposed to vacuum conditions will be severely degraded due to lubricant leakage and removal of the surface oxide layer. Several development programs are currently investigating vacuum-bearing phenomena but no clear-cut answer as yet is available.

b. Electromagnetic Radiation - The space vehicle will be exposed to varying amounts of electromagnetic radiation emanating from the sun, earth and other planetary bodies. During a satellite orbit for example, thermal and albedo radiation from the earth

and the darkness encountered in the earth's shadow will results in temperature variations which might cause distortion, thermal fatigue, and other degrading effects. It currently appears that with large flat structures such as are used in solar power systems this problem can be alleviated by the proper use of reflective coatings.

Limited testing of plastics under ultraviolet radiation has indicated some deterioration is probable for plastics exposed to the UV and X-ray portion of the solar spectrum. A major effect encountered during testing in the earth's atmosphere is oxidation, and recent experiments have indicated a much greater tolerance of organic polymers to high energy photons in a vacuum environment. Major effects in vacuum, spearate from vacuum-thermal volatization, would be increased brittleness, lack of adhesion to substrate, flaking and discoloration due to molecular crosslinking.

Selected epoxy resins have shown great strength under nuclear reactor radiation. Furthermore, increased tolerance of radiation can be obtained by the use of inorganic fillers and protective covers. However, until the magnitude of deterioration is proven, it would not be wise to use plastic materials directly exposed to the sun.

Protected support structures of plastics might be of use. Intensive radiation may increase the amount of peeling of the skin, plastic shrinkage, and other effects which tend to distort structures. Inorganic materials, such as steel or aluminum, can

be used with negligible effects from short wavelength radiation.

An additional source of high energy photons will result from secondary emissions due to high energy particles contained in the Van Allen belts. Available measurements from space probes and satellites indicate that the damage threshold of about 10^8 to 10^{10} rads will not be exceeded for years when exposed to the most intense particle bombardment existing in the inner belt. This threshold may be exceeded, however, by the solar plasma bombardment.

c. Corpuscular Bombardment - An exposed surface may be eroded by sputtering due to the large number of low energy atomic and molecular particles existing in the earth's exosphere, solar plasmas, Van Allen belts, and other sources. In many cases, the spectrum of particle densities and energy can only be guessed from indirect evidence. For example, the number and density of low energy particles trapped in the Van Allen belts has not been measured.

One effect of importance is the decrease of surface coating thickness due to sputtering and physical erosion by the particles. The limited experimental evidence available regarding sputtering effects differs by orders of magnitude in the variation of sputtering yields with target material, particle energy and type, angle of incidence, and other effects.

Use of the most pessimistic assumptions regarding the density and velocity distribution of important chemical species in the

interplanetary gas as a function of time and solar activity (estimates differ by orders of magnitude) results in the removal of up to 8000 Å of aluminum material in a year's time. Reasonable assumptions result in the removal of only 100 - 500 Å. This removal will be evenly distributed over the surface. The effects of sputtering by low energy particles appear not to be serious unless coatings of less than perhaps 1-micron thickness are used. Furthermore, sputtering resistant coatings could probably be developed.

d. Meteoroid Bombardment - An exposed surface in space will be eroded due to meteoroid bombardment. Weak structures might be distorted due to puncture and structural damage. Also, thin skin containers might be punctured and release working fluids. No direct experimental evidence is presently available on the numbers, composition, or effect of the large numbers of small meteoroids present in space, and estimates of surface deterioration rate and/or puncture probability can vary by orders of magnitude.

Using the most pessimistic assumptions the amount of surface coating and surface destroyed during a year's period will be less than 1 percent. It does not appear that meteoroid bombardment will seriously affect system performance during the operational life of a vehicle except where poor design allows the chance puncture of a thin skin to destroy a sensitive component (i.e., hydraulic working line).

Lack of experimental evidence hampers the validity of the discussion of environmental effects and in many cases calculated effects are based on extrapolation and indirect evidence. No experimental evidence exists regarding the effects of the total combined space environment and this lack may possibly lead to serious errors in estimating system degradation.

1.0 VACUUM EFFECTS

At orbital altitudes the pressure (reduced to equivalent density at toom temperature), is approximately 10^{-8} mm Hg at 200 miles and less than 10^{-12} mm Hg at 1,000 miles. These are two important effects on solid materials which occur in a high vacuum. First diffusion and evaporation of volatile components are enhanced by the absence of surface vapor to maintain chemical and physical equilibrium.

The second important effect is the partial or complete removal of the surface film of gas which covers all material in a sea level atmosphere. The effects of surface gas removal are relatively unexplored although some properties such as friction and creep rupture time are known to be significantly changed. This lack of knowledge is due primarily to the difficulty of maintaining an adequate vacuum during tests.

The vacuum required for simulation depends on the material and phenomena involved. Material evaporation simulation requires pressures below 10^{-6} mm mercury to insure a mean free path much larger than the structure. Simulation of surface effects requires much lower pressures, below 10^{-9} mm mercury if possible. For example, kinetic theory indicates

that a monomolecular layer of nitrogen will form in a time given by:

$$t = \frac{(.16 \times 10^{-5})}{P \text{ (mm Hg)}} .$$

Equivalently, 1600 seconds are required to form a layer at 10^{-9} mm Hg.

1.1 Effects of Surface Gas Layer Removal

In a normal sea level atmosphere, every material surface is covered with a thin layer which usually includes oxide and nitrides of the base material as well as physically absorbed gas molecules. This surface layer tends to evaporate in high vacuum and volatilization will be accelerated by incident radiation on the surface layer. The equilibrium situation eventually reached is essentially a perfectly clean surface, a state which is totally unfamiliar in laboratory experiments. Two clean surfaces in contact have a strong tendency to cold weld together at the very small areas or points that actually touch each other. The individual metal atoms, seeing no barrier of foreign material, share bonds and a diffusion of atoms can take place.

An unverified but logical explanation of fatigue failure is the assumption that micro-cracks form at the surface (region of highest stress) during loading. At high pressures oxidation of the freshly exposed surface is quite rapid and healing of the crack is prevented. The crack progressively enlarges until failure results. This explanation is given support by the experimental behavior of chemically inert materials, such as gold, whose fatigue life seems to have little dependence on surrounding pressure. This is shown in Figure I-B-1, which displays the fatigue life of copper, aluminum, and gold vs. air pressure. Many materials exhibit similar increased fatigue life at lower pressures. The effect of space

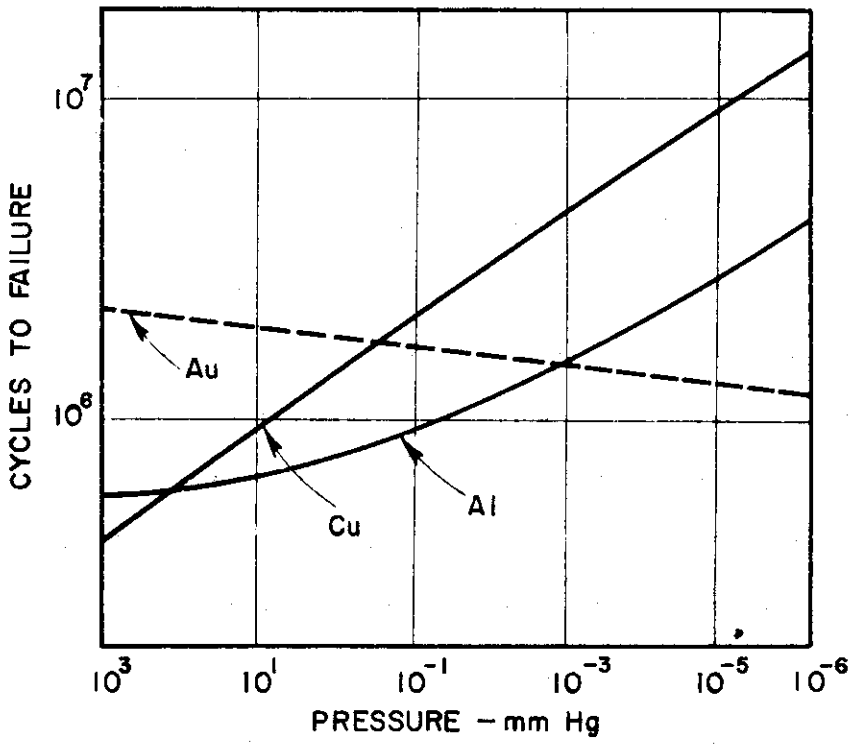

FIGURE I-B-1 FATIGUE LIFE OF VARIOUS METALS VERSUS PRESSURE OF AIR

conditions on the fatigue life properties of materials is unknown but no difficulties are anticipated.

It has been demonstrated in experiment that the test atmosphere, air or vacuum, appreciably affects the high temperature creep rupture properties of metals. At high temperatures and low stresses, creep specimens are stronger in air than in vacuum, but at low temperatures and high stresses, there is a reversal, they are stronger in vacuum. Furthermore, there may be a reversal in the relative creep strength during the course of the test. In the early stages a specimen tested in air may have the better creep resistance while later on there is a reversal and the specimen in vacuum has the lower creep rate. Very often instances of reversals in rates of processes are explained by the simultaneous operation of two competing processes. In the present case, it has been proposed that oxidation strengthens the metal but that absorption of gases weakens it by lowering surface energy and thereby facilitating crack propagation. Since the surface energy of the material is less in an oxygen atmosphere, it is possible that in air crack propagation is facilitated and, after cracking is initiated, the air specimen starts to creep at a faster rate than the one in vacuum and fails sooner. The changes in material strength are generally not of a magnitude large enough to affect component design.

1.2 Evaporation and Diffusion

Below air pressures of about 10^{-4} mm mercury the molecules which leave the surface have a negligible chance of returning and evaporation will be proportional to the vapor pressure.

Table 1 gives the temperature for several evaporation rates for many common metals and semiconductors. The rate of evaporation of an alloy component is reduced by approximately the molecular fraction of that component present. Table I-B-1 indicates the undesirability of depending on magnesium, zinc, cadmium, the alkali metals, or alloys for thin lightweight structures. Aluminum exhibits negligible evaporation at the anticipated temperatures of operation. Nickel, aluminum, stainless steels, and other common structural materials will not be significantly affected. It appears that a wide choice of inorganic materials is available for mirror construction.

Experimentation with organic materials such as plastic films has indicated that few plastics are currently available which can withstand the space environment and still maintain dimensional stability. Vacuum-thermal degradation of various organic polymers commonly used in plastic films and protective coatings has been found to be severe. However, in many cases the percentage of weight lost has been less or only slightly more severe than would occur in a normal sea level atmosphere. Whereas oxidation is the most important factor affecting the stability of most organic polymers in air, bond dissociation or ionization appears to be the determining factor affecting thermal stability in vacuum.

Many of the studies made on vacuum pyrolysis of organic polymers has been accomplished using coatings on a solid substrate. The study of thin films attached to a rigid substrate where the film may be under considerable stress would probably give much different results. Also, the far ultraviolet radiation in the space environment will enhance volatization and serve to increase mechanical degradation of the plastic material. Much work remains in the analytical and experimental evalu-

TABLE I-B-1

EVAPORATION OF METALS AND SEMICONDUCTORS IN HIGH VACUUM

Element	Temperature (°F) at which evaporation is 10^{-5} cm/yr	10^{-3} cm/yr	10^{-1} cm/yr	Melting Point °F
Cd	100	170	250	610
Se	120	180	240	430
Zn	160	260	350	790
Te	260	350	430	840
Mg	260	350	460	1200
Li	300	410	530	370
Sb	410	520	570	1170
Bi	470	600	750	520
Pb	510	630	800	620
In	760	940	1130	310
Mn	845	1010	1200	2300
Ag	890	1090	1300	1760
Sn	1020	1220	1480	450
Al	1020	1260	1490	1220
Be	1140	1300	1540	2340
Cu	1160	1400	1650	1980
Au	1220	1480	1750	1950
Ge	1220	1480	1750	1760
Cr	1380	1600	1840	3440
Fe	1420	1650	1920	2800
Si	1450	1690	1970	2580
Ni	1480	1720	2000	2650
Pd	1490	1720	2020	2840
Co	1500	1760	2020	2720
Ti	1690	1960	2280	3140
V	1870	2150	2460	3100
Rh	2080	2420	2800	3580
Pt	2120	2440	2840	3240
B	2240	2580	2980	3720
Zr	2340	2740	3150	3360
Ir	2380	2740	3150	4450
Mo	2520	2960	3450	4700
C	2780	3050	3400	6600
Ta	3250	3700	4200	5400
Re	3300	3700	4200	5700
W	3400	3900	4500	6100

ation of the combined vacuum-thermal-ultraviolet environment.

High polymers are lost in vacuum due to the breaking down of chains into smaller fragments. One analytical theory is that of random degradation, in which all of the chain links between monomer units are assumed to be of equal strength and accessibility, and thus can break at random anywhere in the polymer chain, resulting in various sized fragments. A variation of this theory assumes that some of the links are more easily broken than others. Breakdown is often accelerated by the addition of a small amount of impurities.

Another theory is called a reverse polymerization process, implying the reverse of the step-wise polymerization process that formed the polymer chain. This is a chain reaction process which occurs in the following steps: initiation, propagation and termination. Initially free radical ends may be formed by the breaking away of such foreign particles as oxygen and water or by the breaking of the polymer chain. This may occur at random, at weak links, only at the chain ends caused by the splitting off of monomer units, or the scission may be caused by the catalyst incorporated in the chain during the polymerization. It has been found that the catalyst which promotes polymerization can also catalyze depolymerization. As these free radicals become activated, monomer units may begin splitting off the chain ends in rapid succession by a propagation or unzipping reaction until the polymer chain is destroyed or the propagation is terminated. The termination reaction may result from coupling, disproportionation or chain transfer. Coupling implies the collision and combination of any two free radicals. Disproportionation is a mechanism by which one free radical extracts the hydrogen atom from another radical resulting in two stable molecules. The chain transfer mechanism consists of a free radical abstracting an atom from another molecule forming a stable chain and a new radical.

Degradation can be measured quantitatively by the loss in weight of a material during a given exposure time under vacuum conditions. Weight loss is partially due to the volatilization of hydrogen, oxygen, water, carbon dioxide and other breakdown products. Another measure of degradation is the tensile strength and elongation characteristic of film

samples after vacuum exposure. These preliminary tests, however, are suitable only for initial selection of plastic materials. These simple measurements do not provide any measure of the interaction of plastic structural elements, i.e., support structure, skin, etc. Such effects as shrinkage, orange peel, deterioration of adhesives, separation of a plastic skin from its support and other effects which may severely degrade performance can only be ascertained when an entire structure is placed in a combined vacuum-thermal-ultraviolet environment.

The weight losses suffered by various films in tests using temperatures ranging from ambient to 600°F are reported in the references. The results of a typical test of this type are shown in Figure I-B-2, which shows the step-wise weight losses of various organic polymers under vacuum at various temperatures. The amount of degradation and the mechanism can be generally related to the class of polymer used and its molecular structure. For example, polyester polymers suffer from random degradation due to the ionization or disassociation of the weak ester linkage. In this case materials containing ester, ether, amide, etc. linkages would probably be unsuitable for a vacuum-thermal environment unless perhaps both sides of the linkage consisted of groups too large to volatize. Other examples of this type can be found in literature but the great majority of organic polymers remain to be investigated and only a few cases of interest will be presented here. Table I-B-2 shows an estimated order of merit for behavior of plastics in vacuum, with temperatures where the calculated weight loss is 10 percent/year, subject to considerable uncertainty depending on the quality of the experimental data.

TABLE I-B-2

ESTIMATED ORDER OF MERIT FOR BEHAVIOR OF PLASTICS IN VACUUM

POLYMERS	Temperature for 10 percent weight loss per year in vacuum °F.
Styrene	80 - 270
Nylon	80 - 340
Methyl methacrylate	80 - 390
Sulfide	100
Cellulose nitrate	100
Cellulose, oxidized	100
Methyl acrylate	100 - 300
Ester	100 - 460
Epoxy	100 - 460
Urethane	150 - 300
Vinyl butryl	180
Vinyl chloride	190
Linseed oil	200
Neoprene (chloroprene)	200
Alkyd	200 - 300
Acrylonitrile	240
Styrene-butadiene	270
Phenolic	300 - 510
Vinyl alcohol	310
Vinyl acetate	320
Cellulose acetate butyrate	340
Hydrocellulose	350
Cellulose	350
Carbonate	350
Methyl styrene	360
Cellulose acetate	370
Rubber, natural	380
Isoprene	380
Isobutylene-isoprene (butyl rubber)	380
Melamine	380
Silicone rubber	390
Ethylene terephthalate (mylar, dacron)	400
Isobutylene	400
Vinyl toluene	400
Styrene, cross-linked	450
Butadiene-acrylonitrile (nitrile rubber)	450
Butadiene-styrene (Gr-S = SBR)	460
Vinyl fluoride	460
Propylene	470
Butadiene	490
Chlorotrifluoreoethylene	490
Ethylene, low density	490 - 540
Chlorotrifluoroethylene-vinylidene fluoride	500
Vinylidene fluoride	510
Benzyl	540
Xylylene	540
Ethylene, high density	560
Trivinyl benzene	560
Tetrafluoroethylene	710
Methyl phenyl silicone resin	720

Of the many materials investigated many of them withstood the vacuum environment at ambient temperature without significant weight loss. Mylar is one of these. In addition, several materials (polyester, vinyl copolymer and neoprene) cracked and partially flaked off in tests conducted at 200° F.

A solar mirror which absorbs 10 percent of the incident solar radiation (130 watts/ft^2) will achieve skin equilibrium temperatures ranging between 250 and -50°F depending upon the effectiveness of the heat conduction away from the skin to the rear surface of the mirror. Secondary mirrors used for reflection of concentrated sunlight will maintain higher equilibrium skin temperatures. For example, if a small mirror reflects concentrated solar radiation equivalent to 10 times the solar constant, skin equilibrium temperatures will range between 800 and 250°F, again depending upon the effectiveness of heat conduction from the skin.

Examining Table I-B-2, several materials appear stable up to 250°F. One interesting case shown in Figure I-B-2 employed a barrier coat of a silicon polymer on a less stable silicon alkyd. This coating reduced the volatilization by more than 50 percent over a wide range of temperatures. As a rule of thumb, polymers should not be selected for use at temperatures above those recommended for use in air; maximum temperatures for service in air are available in handbooks, specifications, and manufacturers' literature.

Plasticizers and mold lubricants are also highly detrimental to stability in vacuum. The particular formulation and curing procedure used may, therefore, have important effects upon vacuum stability as has been demonstrated in several experiments. For support structures, the loss of material may be significantly less. The movement of the plasticizer inside the polymer is a diffusion process which may be much slower than the loss from the surface. It can be shown that this loss from a slab-shaped piece of material proceeds approximately as:

R-AMBIENT TEMPERATURE RUN; 2-200°F, 3-300°F,
4-400°F, 5-500°F

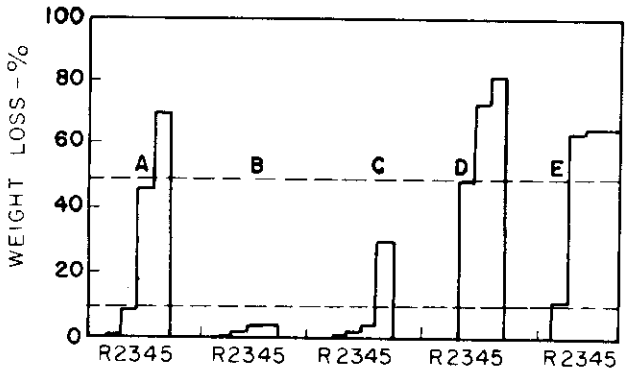

A polyvinl bu Tyral
B Kel-F 820
C cell-acet-butyrate
D nitrocellulose
E polysulfide

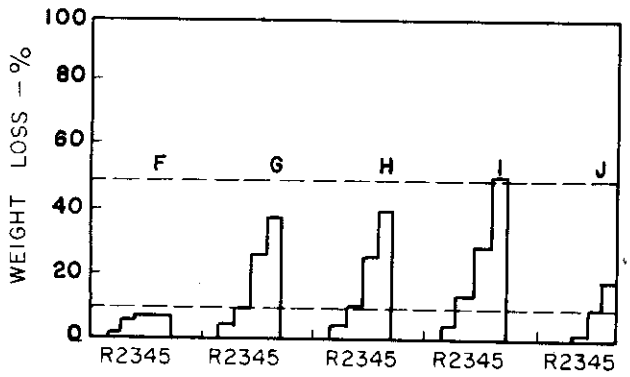

F phenolic
G silicone alkyd-1 mil
H silicone alkyd-2 mil
I silicone alkyd-8 mil
J silicone over silicone alkyd

FIGURE I-B-2 STEPWISE WEIGHT LOSSES OF VARIOUS ORGANIC POLYMERS UNDER VACUUM

$$P = P_o e^{-t/T}$$

P = Amount of plasticizer per unit area of slab in material at time t

P_o = Amount initially present at t= 0

T = Time constant related to the diffusion constant

The inhibition of volatilization could be accomplished by covering the support structure. It should be noted that after launch and erection, structural stability may not be nearly as important a criterion for high performance as dimensional stability. Thus, a great loss of material could be endured if side effects such as shrinkage or flaking did not occur. It is also of interest to note that the majority of weight loss occurs in a short time period.

As an example, a typical polyurethane foam at 400°F lost 20 percent in 4 hours, 44 percent in 24 hours, 50 percent in 48 hours and 60 percent in 72 hours. This rapid loss of material indicates that any tests undertaken in space to ascertain the effects of environment could be run quickly. Also, measurements taken over a short period in a simulated atmosphere can be misleading.

The operation of bearings exposed to a space environment will suffer due to evaporation of any lubricants used and increased friction due to surface gas removal. At the present state-of-the-art no foolproof seal or dry bearing has been developed.

If possible, the best way to overcome the in-space lubrication problem is to seal the bearings. If this is not feasible the usable lifetime of the bearing lubricant can be increased by shrouding the bearing in such a way that evaporative lubricant molecules will not be lost entirely. It is of course desirable to use low vapor pressure oils and greases such as the types used in diffusion pumps. Petroleum based oils may be slightly better

in this regard than silicon oils. The use of dry lubricants probably offers more promise than liquid lubricants. Graphite is unsatisfactory even at the altitudes encountered by present day aircraft. Molybdenum sulfide, however, may be satisfactory if properly applied. The grade used is also quite important. It should be bonded to the substrate possibly by means of a non-evaporating resin.

Another approach involves thin metallic bearings such as are used in rotating anode X-ray tubes. Silver is a common material for this application. The difficulty with this approach is that the bearings probably will not work in air and this complicates the manufacture and test problem. Testing must also be done in an extremely good vacuum as much of the lubricating effect depends on the presence of a monomolecular film of gas on the material surface.

2.0 ELECTROMAGNETIC RADIATION

A vehicle structure will be bombarded by electromagnetic radiation from several sources including direct solar radiation, Albedo, earth and atmospheric low temperature radiation, reflected and thermal radiation from the surface of a satellite, and interplanetary radiation.

A thermal equilibrium of power systems structures such as a solar concentrator or array of photovoltaic cells will vary according to the variations in earth Albedo and thermal radiations, and periods of darkness encountered during satellite orbits. A typical example of the radiation inputs to a flat plate which is continually oriented towards the sun during a satellite orbit of 100 minutes (500 miles) is shown in Figure I-B-3. In this example, incident radiation from sources other than the sun vary from 820 watts/meter^2 at "noon" to 140 watts/meter^2 when the satellite entered the earth's shadow.

The equilibrium temperature of a large flat structure will depend on the reflective and emissive properties of the front and rear surfaces. In general, structures which maintain continuous orientation towards the sun will minimize thermal gradients and maintain minimum temperatures when surface emissivities are high between .95 and 1.

The satellite will encounter varying periods of darkness depending on the orbit altitude, time of year, orbital inclination, and related factors. This is clearly shown in Figs. I-B-4 and I-B-5.

Of greatest importance in estimating degradation of structures in space is the UV and X-ray part of the solar spectrum. While the visible and infrared spectrum approaches a black body distribution with equivalent

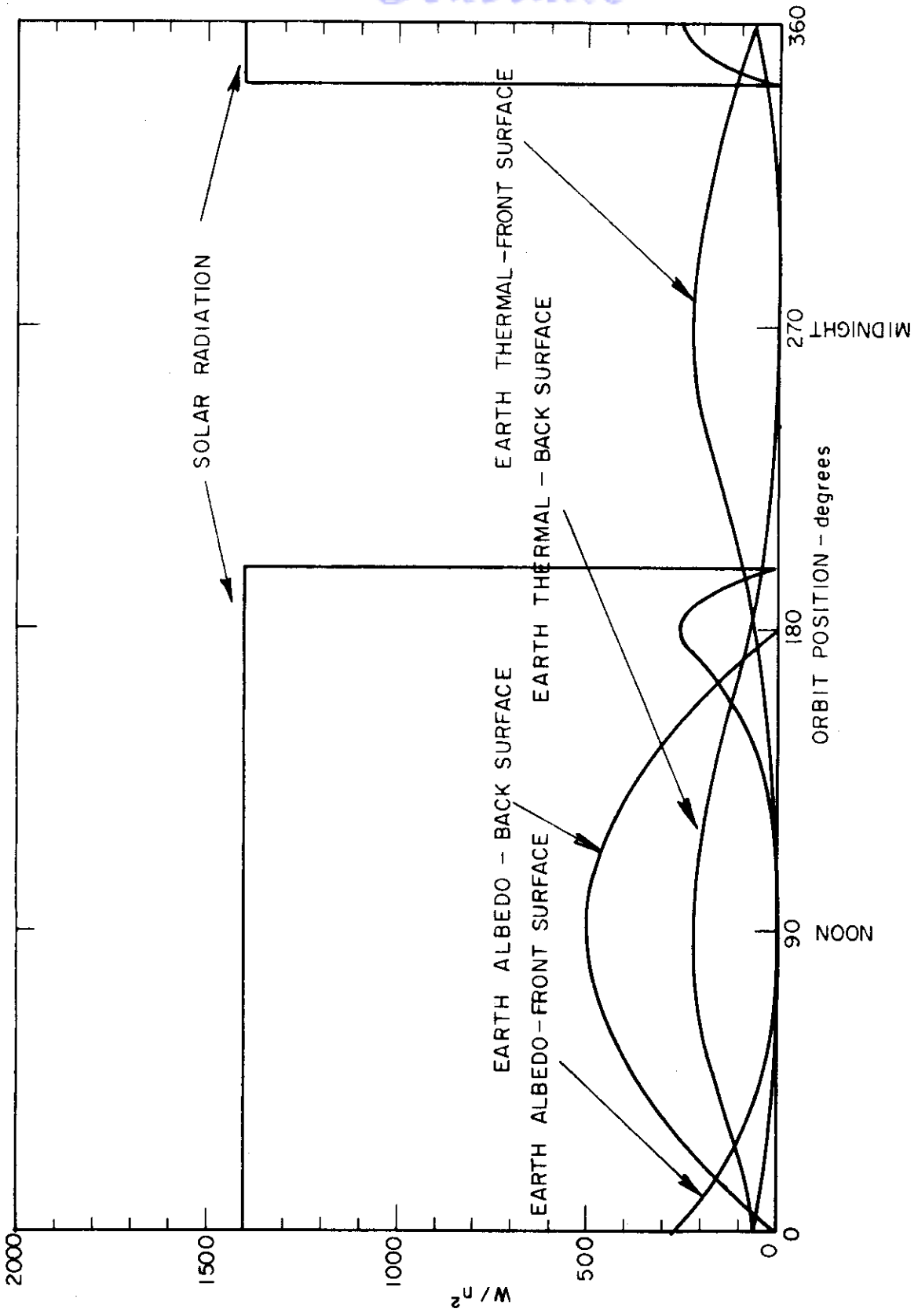

FIGURE I-B-3 HEAT INPUTS TO A FLAT PLATE DURING A 500 NAUTICAL MILE SATELLITE ORBIT

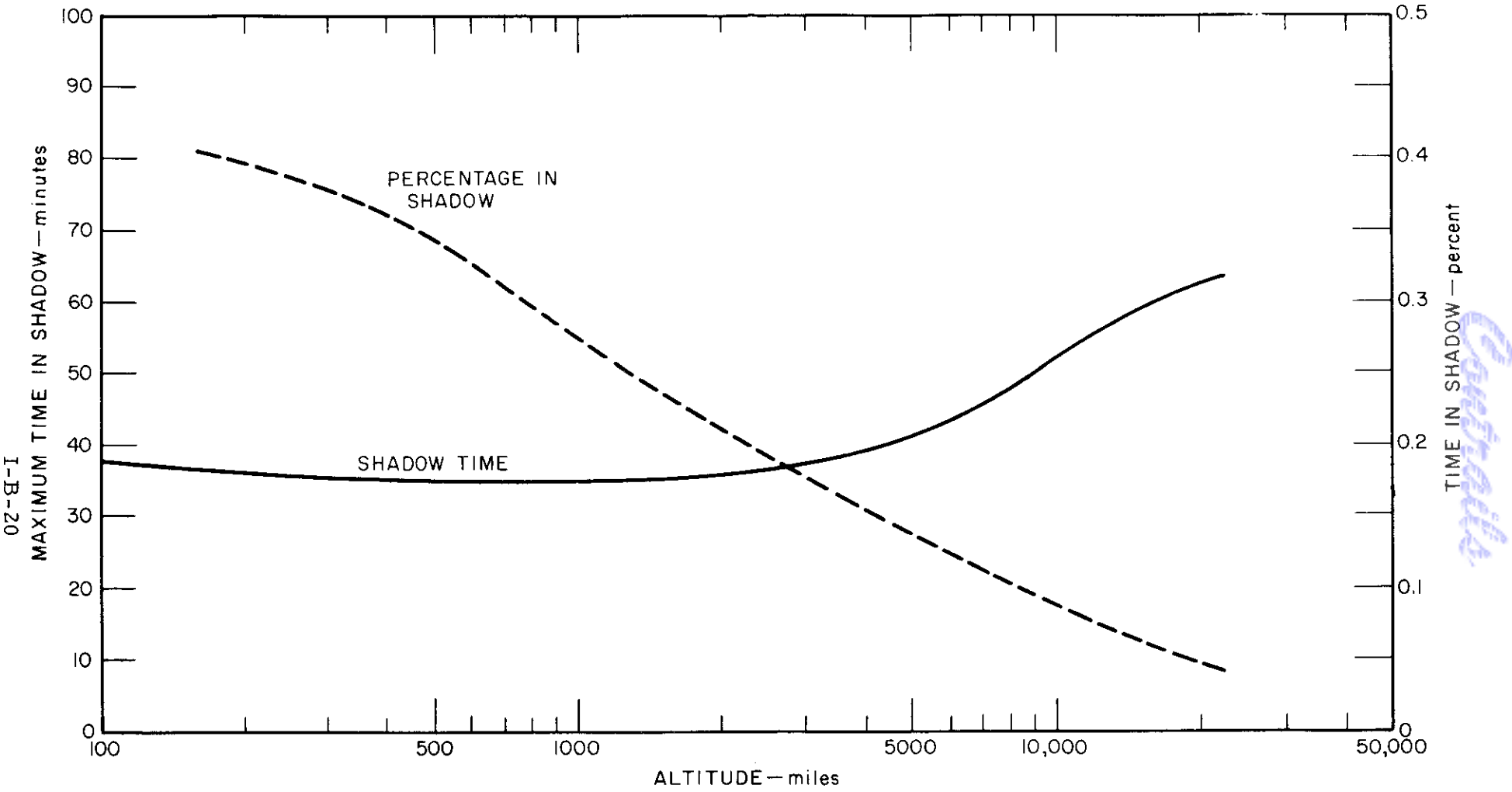

FIGURE I-B-4 MAXIMUM TIME IN SHADOW OF SATELLITE

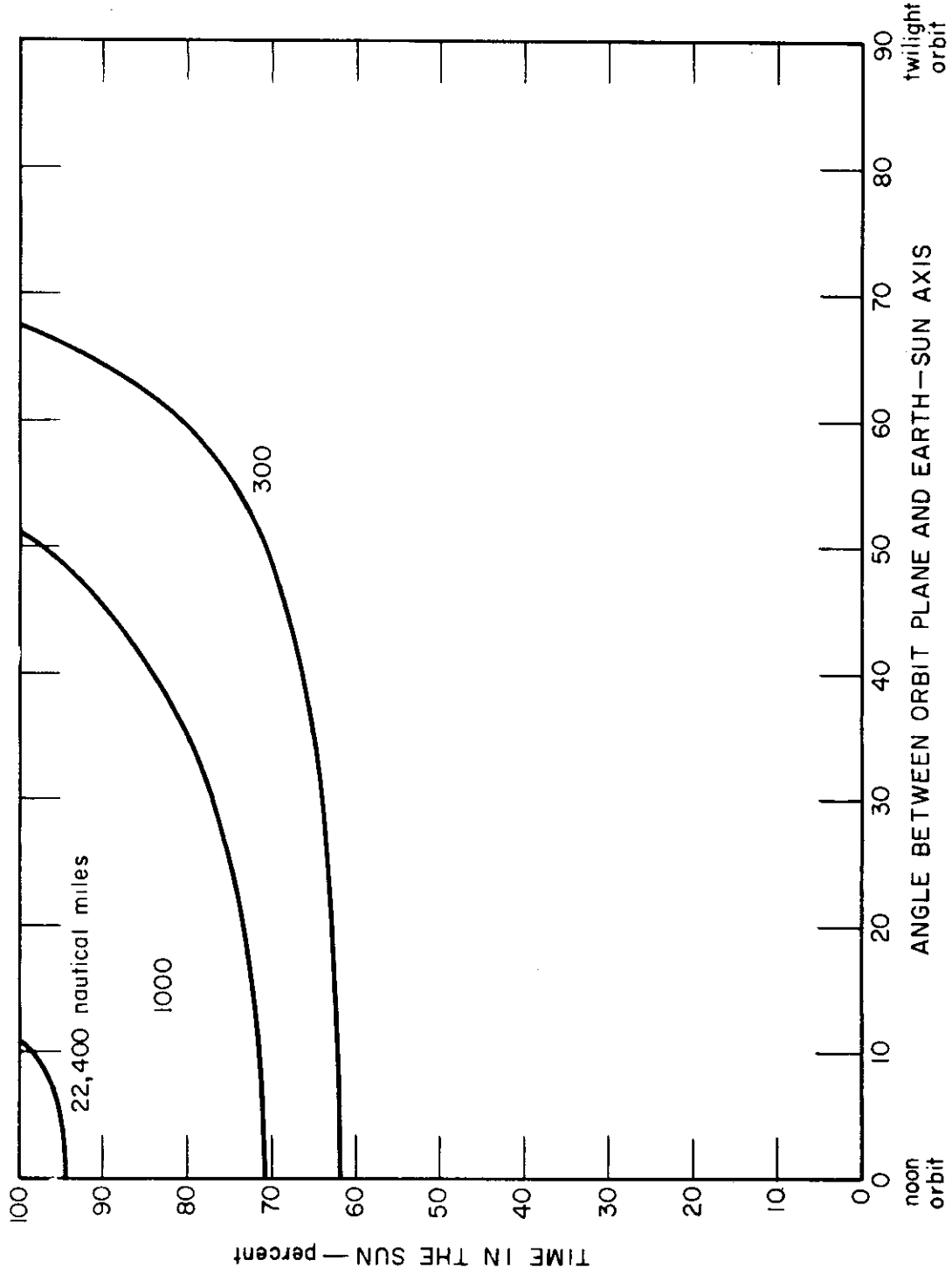

FIGURE I-B-5 PERCENT TOTAL ORBIT ILLUMINATION VERSUS ANGLE BETWEEN ORBIT PLANE AND EARTH-SUN AXIS

temperatures of about 5700° K, the UV and X-ray regions are orders of magnitude higher. The energy in the Layman -H_α line at 1216 Å is much more intense than the ultraviolet continum, perhaps reaching values of 1μ w/cm^2 as shown in Fig. I-B-6. This line intensity corresponds to a high equivalent black body temperature which may come from hydrogen in the chromosphere of the sun, where the equivalent temperature can rise to the order of 100,000°K. The total energy contained in the 0-2200A region is approximately 30μ w/cm^2 during a "quiet" sun. An estimated distribution is given in Table I-B-3 below.

Table I-B-3

Solar Energy Distribution

Wavelength Region	ergs cm^{-2} sec^{-1} per Wavelength Interval at Mean Earth Distance
0-1A	$< 10^{-5}$
1-8A	$< 10^{-3}$
0-100A (x-region)	~ 0.1
100-1000A	< 10
1000-1350A	< 10
L_α line at 1216A	~ 6
0-2200A	< 300

The lack of experimental evidence produces a great uncertainty in the magnitude of the X-ray emission. The region below about 100 Å changes

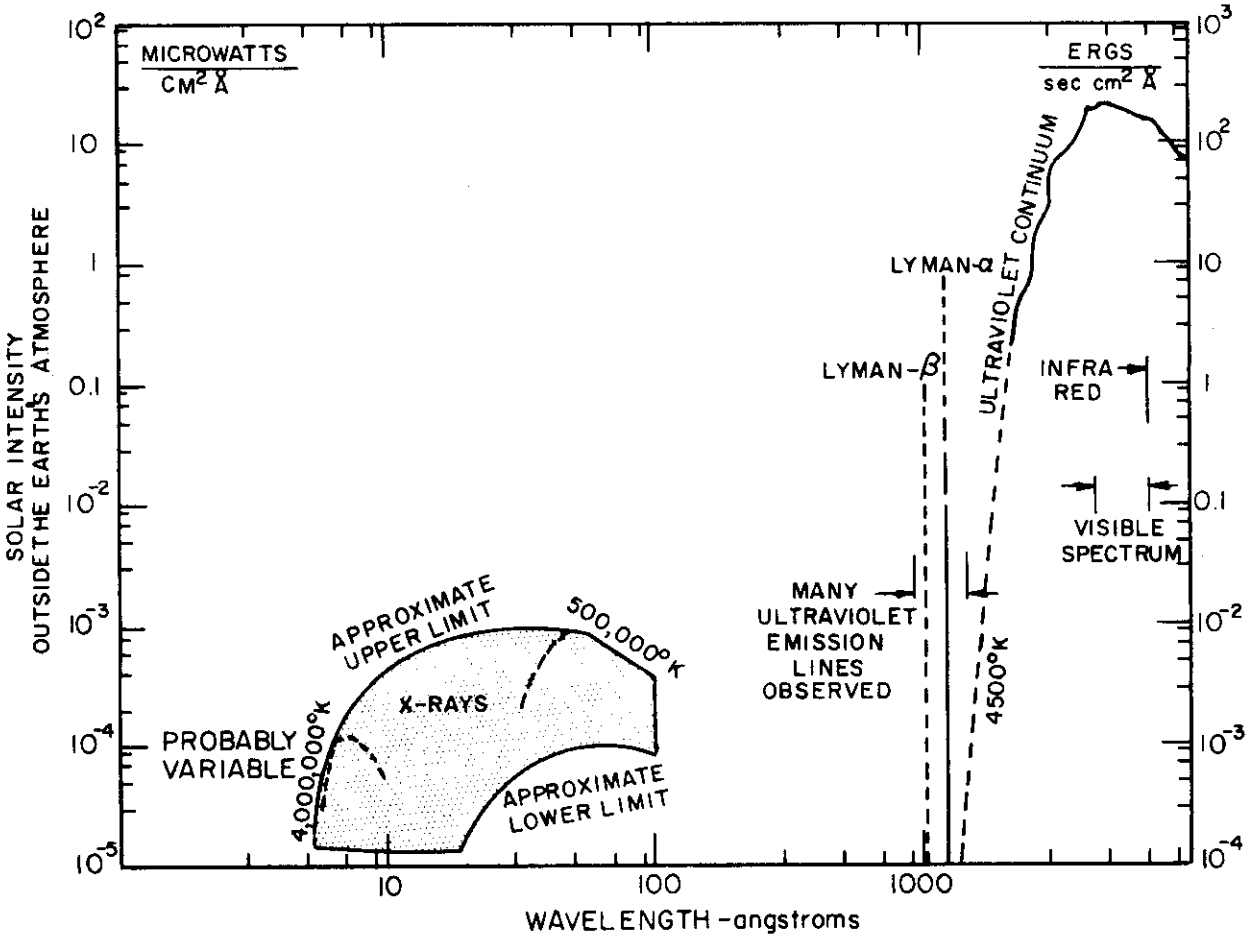

FIGURE I-B-6 SOLAR ELECTROMAGNETIC SPECTRUM

significantly with solar activity with several wavelength regions changing by a factor of 10^2 to 10^5 during solar flares. Normal flares last for a few hours and occur about 10 times per year. There also exists a gap from 100 to 950 angstroms due to the lack of instrumentation.

Near ultraviolet and far ultraviolet radiation, in general, has less effect upon the behavior of plastics in vacuum than air. Accordingly, arguments are found in the literature stating that behavior under normal daylight on Earth, in air, should provide a safe guide to effects of ultraviolet in space. Until the magnitude of space radiation and the effects of hard UV and X-ray (absent on Earth) are ascertained, however, the issue will remain in doubt.

Limited testing of plastics under ultraviolet radiation in the atmosphere has indicated possible serious consequences. For example, a radiation dose of 0.1 wh/cm^2 on a specimen of 1/2 mil transparent Mylar film, with radiation in the region from 3,120 to 3,320 angstroms, produced striking results in the bulk properties of the Mylar. At -70°C stress was reduced by a factor of 2 (20,000 to 11,000 psi). Material receiving an integrated dose of 0.2 wh/cm^2 became too brittle to be handled at low temperatures.

Degradation suffered by the material was dramatically illustrated by a falling ball test. When a falling ball was dropped through a sample of the Mylar which had been sufficiently exposed, the resulting tear was identical to a brittle shatter exhibited by extremely cold plastics.

The space solar intensity in the region of 3,120Å to 3,320Å is approximately 8μ w/cm^{2}Å. These results indicate, therefore, that clear 1/2 mil Mylar film held at cold temperatures would become extremely brittle in a matter of 60-100 hours exposed to just a small portion of the solar spectrum. The integrated energy over the ultraviolet and X-ray region, however, will be several orders of magnitude higher, and the rate of embrittlement and change of material properties will be correspondingly higher.

A number of plastic materials have been tested under reactor irradiation. These materials have shown wide variation in resistance to irradiation in terms of structural properties and other effects. Polystyrene, mineral-filled polyesters, asbestos-filled Furan, asbestos-filled phenolic, and Fiberglas laminated plastics, for example, have been shown to be quite resistive to irradiation. Second in desirability are such materials as polyethylene, Mylar, and others of a similar nature. Nylon, natural rubber, and celluloid plastics are of medium resistivity, while Teflon is very poor. As an example, the life of the best material, polystyrene, used in an insulating capacity, would be over 10^4 times the life of the poorest material, Teflon. The results of reactor testing can be used only as an approximate indication of the resistivity of the materials to the ultraviolet and X-ray regions of the solar spectrum. Results of these tests can be obtained from the Radiation Effects Information Center of Battelle Memorial Institute.

Experiment has shown that the use of inorganic fillers in plastic serves as an impediment to irradiation deterioration. Another protective measure would be the coating of the plastic with an inorganic material such as aluminum. Reflectivity of a mirror coating of aluminum of 600Å thickness has been given as about 0.92 at wavelengths from 4000Å to 2000Å under ideal conditions. The radiation reaching the plastic has been calculated to be only about 10^{-13} of the incident radiation for this coating thickness. The reflectivity of films between 500 and 2000 angstroms has been shown to decrease, as the irradiating wavelength decreased, to values of 0.13 at 900Å. The effect of aging also increased strongly with decreasing wavelength, with reflectivity decreasing from 0.2 to 0.004 in one year in this region. This decrease, however, was attributed mainly to formation of an oxide layer. Despite low reflectivity, transmission is probably quite low because of the high absorptivity. For example, the transmissivity of a coating 1350Å thick has been given at about 0.001 at wavelengths between 1250 and 830 angstroms.

In the 900Å to 300Å region transmissivity decreases rapidly. For example, a 500Å thick coating has transmissivity of 0.01 at 833Å and 0.5 at 500Å.

For normal coatings, therefore, wavelengths longer than 833 angstroms might not reach the plastic material; but a considerable fraction (close to 10 percent) of wavelengths of 500Å might penetrate to the plastic. It would be expected, therefore, that aluminum coatings would have little protective effect in the X-ray and hard ultraviolet regions.

Experiments which directly compared the degradation encountered in normal laboratory atmospheres compared to vacuum have indicated that the high rate of polymer film degradation usually associated with the effects of ultraviolet light depend upon the presence of an oxygen bearing atmosphere. Initial studies point to the probability that in most instances polymers will degrade less rapidly in vacuum than in air, the formation of volatile products and consequent weight loss being significantly less.

Molecular crosslinking was observed to occur within films during vacuum-ultraviolet exposure. Excessive crosslinking will result in brittleness, shrinkage and loss of adhesion to a substrate material. For example, 80 hour exposures of vinyl chloride and methyl methacrylate films in vacuum, with intensities of 1 mw/cm^2 in the region 100 to 3,000Å, induced no changes that were detectable by infrared spectroscopy. However, the irradiated films were discolored and neither film could be dissolved from the holding plates although both were readily soluble before irradiation. Similar films exposed to a normal laboratory atmosphere experienced severe decomposition.

The accumulated evidence indicates that plastic films and supporting structures can be developed that will successfully resist the short wavelength electromagnetic radiation existing in space, particularly when coatings in organic fillers and other protective mechanisms are used.

Based on experience gained in the reactor irradiation of materials, it is not expected that or other electromagnetic radiation will have significant consequences on the integrity of any structure using aluminum or other common inorganic structural materials.

High energy corpuscular radiation in the Van Allen radiation belts will produce secondary emissions in the short wavelength region which could be particularly penetrating.

The consequences of proton bombardment are dependent upon the energy. At lower energies gamma flux is released when the nucleus returns to its ground state. At high energies, (greater than 150 mev) intermediate mass particles, mesons, are generated and then decay with resultant gamma photons. Electrons in the process of losing their energy in the first layers of skin will generate considerable Bremsstrahlung radiation. The peak intensities in each radiation belt resulting from these proton and electron nucleus interactions equals about 10 roentgens per hour normally.

The damage threshold for most organic polymers lies in the range of 10^8 to 10^{10} roentgens. It appears, therefore, that secondary radiation resulting from Van Allen belt interaction will not seriously degrade plastic materials. During increased solar activity, maximum intensity in the outer zone will increase by a factor of 10-100 over the maximum on quiet days. The intensity buildup over a period of 12 hours during the August 1959 solar flare equaled 500 roentgens per hour. It remained at this level for 12 more hours and required four to five days to reach a safe level. The short lifetime of these flares prevents them from becoming a serious degrading factor.

Other secondary emissions will result from bombardment by protons and electrons in the solar plasma (see Section 3). Proton energy will range between 2 kw and 20 kw. Radiation damage effects would be expected if the surface of the plastic film itself, rather than an overlying metal coating, were exposed to the solar plasma. Radiation damage produced by relatively slow, heavy particles of the kind present in solar plasmas has not been extensively studied. If all the incident proton energy is converted to short wavelength radiation, doses ranging from 5×10^5 rad/sec during "quiet" conditions to 10^8 rad/sec during solar flares from the proton flux alone could be expected. Contributions from heavy particles in the solar stream would range from 3500 to 5×10^5 rad/sec. Therefore, a strong possibility exists that serious radiation damage will result from the solar plasma.

3.0 CORPUSCULAR EROSION

In interplanetary space, i. e., within the solar system, the particles are predominantly of solar origin. The solar corona consists of outstreaming gas which at the earth's distance from the sun is estimated to be between 10^2 and 10^3 protons/cc and an equal number of electrons, both moving with a velocity of about 500 kilometers per second under quiet conditions. During solar flares, densities of 10^4 or perhaps 10^5 protons and electrons per cc moving with a velocity of as high as 1500 km/sec can be expected. The proton kinetic energy in this stream then varies between 2 and 20 kev. Since these energies are much greater than the potential energy of the particles in the solar gravitational field, the concentration of particles will vary inversely as the square of the distance from the sun.

Although not detected, other solar gases may be present in abundance. Since the corpuscular beams appear to be merely segments of the solar corona blown out bodily, both helium and heavier elements can be expected. If it is assumed that no fractionation occurs during the explosive acceleration, it would be reasonable to expect a plasma composition similar to that of the corona itself by weight, roughly 75 percent hydrogen, 23 percent helium, and 2 percent heavy elements. A population ratio of 75 hydrogen to 6 helium atoms might then be expected. The helium would travel at the same velocity as the general proton stream and would, therefore, possess correspondingly higher energies and momentum.

The solar wind through which the earth moves does not penetrate the geomagnetic field. A cavity is formed which contains the earth's magnetic field and atmosphere as graphically illustrated in Fig. I-B-7. The geomagnetic field is severely deformed by the solar wind. Outside the cavity, the gas is principally of solar origin, inside the cavity it is of telluric origin. The boundary is turbulent, and varies from about 6 earth radii in the direction facing the sun and perhaps up to 18 radii away from the sun.

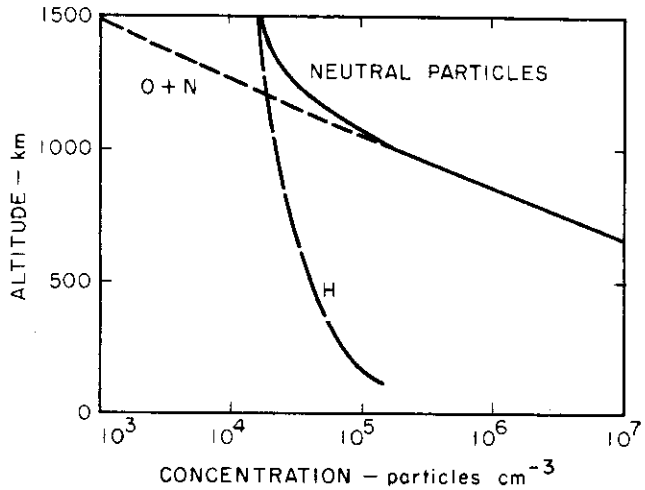

DISTRIBUTION OF NEUTRAL PARTICLES IN THE UPPER ATMOSPHERE

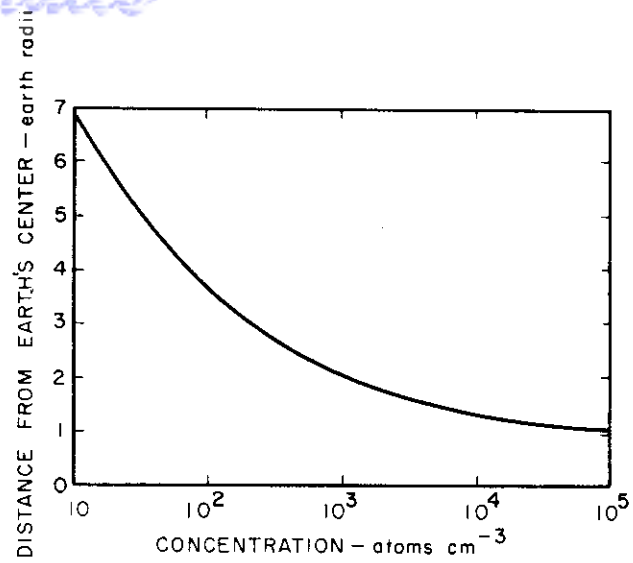

DISTRIBUTION OF ATOMIC HYDROGEN NEAR THE EARTH

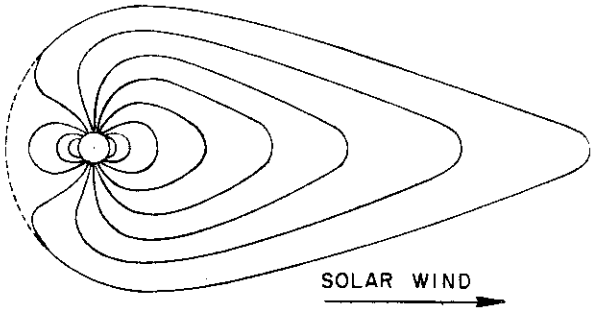

EARTH'S MAGNETIC FIELD AS DEFORMED BY THE SOLAR WIND (BOUNDARIES MUST BE TURBULENT)

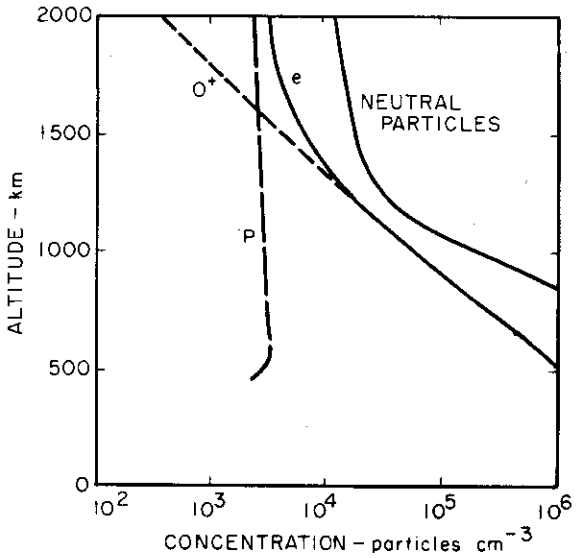

DISTRIBUTION OF IONS IN THE UPPER IONOSPHERE

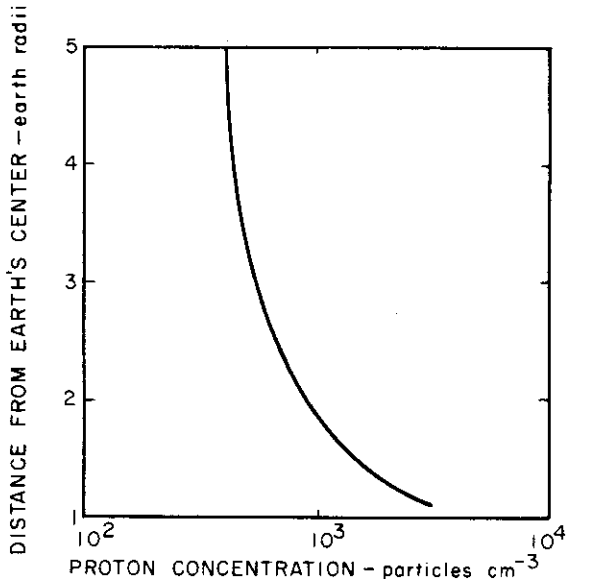

DISTRIBUTION OF PROTONS AND ELECTRONS IN THE PROTONOSPHERE

FIGURE I-B-7 DISTRIBUTION OF PARTICLES NEAR THE EARTH

The concentrations of various atmospheric constitutes are shown in Fig. I-B-7. The oxygen and nitrogen of the earth's atmosphere become dissociated in the ionosphere. At the base of the exosphere, which is a level above which collisions between gas particles can generally be neglected (about 550 km), the gas particles are principally atomic oxygen and atomic nitrogen. As shown in Figure I-B-7 the oxygen and nitrogen concentrations at the base of the exosphere greatly exceed the concentration of atomic hydrogen. Atomic hydrogen, however, does not fall off rapidly with altitude and predominates above 1300 kilometers. The concentration of hydrogen decreases until at 7 earth radii concentration is only about 10 atoms per cc.

The temperature of the hydrogen corona around the earth is the same as the atmospheric temperature at the base of the exosphere or about 1250°K as determined from the rate of orbital decay of the Vanguard satellite. The equivalent energy is .16 ev.

The protons above the base of the exosphere are distributed according to a diffusive equilibrium as shown in Fig. I-B-7. These protons along with an equal number of electrons constitute the protonosphere which is the extreme extension of the ionosphere responsible for the propagation of radio whistlers. The protons and electrons are characterized by the same temperature as the base of the exosphere or 1250°K.

In addition to the atmospheric particles discussed above, both neutral and ionized, there are a few high energy particles to be considered near the earth. The geomagnetic field contains trapped particles which constitute the Van Allen radiation. The trapped high-energy particles are few in number and consist of something on the order of 10^{-6} protons per cc with energies up to 700 mev with a most probable energy of a few mev in the inner zone of the Van Allen radiation belt. There are also about 10^{-4} electrons per cc in the inner zone and 10^{-2} electrons per cc in the outer zone with energies below 800 kev, with the peak of the energy spectrum falling near 100 kev. All of these energy values are considerably in doubt at this time as too few measurements have been made to establish reliable limits. Furthermore, no measurements have been made of the concentration of low energy particles trapped in Van Allen radiation belts.

Other high energy particles contributing slightly to the numbers of particles in "near-earth" space are the cosmic rays and the solar flare protons. The cosmic rays amount to about 10^{-10} particle per cc with energies generally greater than 10^{9} ev. In the vicinity of the solar system and following certain solar flares, the number of energetic particles may increase considerably due to the ejection of solar flare protons with energies on the order of 100 mev and concentrations on the order of 10^{-6} to 10^{-8} protons per cc. These events occur irregularly (5 times in 20 years) and the protons remain in the solar system for only a few days until they become lost.

The effect of primary particle radiation on a surface is relatively unknown. Semi-empirical relations have been derived for the physical sputtering of metals such as given in the equation below which calculates the threshold energy, V_o, for particles of atomic weight, M, impinging normal to a surface of atomic weight, M_s:

$$V_o = \left(\frac{1.6 \times 10^5 \, (M + M_s) \, \phi}{M^{1/2} \, M_s \, W} \right)^2 \quad \text{electron volts}$$

where ϕ = heat of sublimation of the surface material, kcal/mol

W = bulk sound velocity for the material, cm/sec.

This semi-empirical expression was obtained by Wehner and fits experimental observations obtained with thick samples at room temperature or above. Applying these results to the sputtering of very thin structures or coatings by the hydrogen rich solar plasma stream can only give approximate results because:

1. The possibility of chemical sputtering through metal hydride formation which would require much lower threshold energies.
2. Possible differences between thin film properties and bulk mechanical properties which can change the kinematics of momentum transfer.
3. Differences between ionized and neutral atom sputtering mechanisms.

For protons on aluminum, the calculated threshold for perpendicular incidence using a heat of sublimation of 75 kilocalories per mole and a bulk sound velocity of 5.1×10^5 cm/sec is 560 ev. The energy of solar protons outside the earth's magnetic field for 1000 kilometers/sec is 5100 ev. Thus, sputtering thresholds at normal incidence are likely to be exceeded by large margins.

Theoretical predictions and experimental observations on sputtering yield vary widely and values of .05 to over 1 might be appropriate for the given situation. Still higher yields might be appropriate for other than normal incidence.

If the assumption is made that one atom is removed per collision, the total thickness of surface removed can be derived as

$$\Delta t = \frac{NVMT}{\rho N_A}$$

where N = number of corpuscular particles per unit volume
V = average velocity of particles with respect to surface
M = molecular weight of the average surface material atoms
T = time of operation
ρ = density of surface material
N_A = Avogadro's number

As an example, for protons, assuming that N = 1000 cm^3 and $V = 5 \times 10^7$ cm/sec, using an aluminum surface for a period of one year would result in the removal of approximately 0.40 microns of material.

The removal of the material would tend to result in a smooth polishing effect, and optical reflectivity of a mirror surface would be affected probably only where coatings of less than a micron thickness were employed. The possibility of a change in surface quality and decrease in specular reflectivity due to hydride formation and other chemical action is remote.

The presence of heavier particles (e.g., He^+) in the solar stream could lead to appreciable effects. For example, silver has shown a sputtering yield for He^+ higher than for H^+ by a factor of about 9 in the 10 kev region. The sputtering threshold for He^+ drops appreciably due to higher momentum transfer efficiency. This rise in yield would make the sputtering by solar He^+ about equal to that by solar protons.

The average beam of intense protons resulting from solar flares passes the earth in about 10^3 to 10^4 sec. For densities and velocities corresponding to an intense storm (v = 1500 km/sec and N = $10^5/cm^3$) .02 microns would be removed per storm, or about .20 microns per year (plus .20 microns removed by He^+) in addition to the normal erosion.

For ions and gas molecules anticipated at satellite heights of 300 kilometers, if every collision removed 5×10^{-5} atoms, the amount of material removed in one year from an aluminum surface would be approximately 0.55 micron in average depth (assuming N = $2 \times 10^9 cm^3$ and V = 9×10^5 cm/sec).

The figure for proton erosion is probably of the right order of magnitude, as the sputtering threshold energy in most metals is less than 1000 ev. and the energies of the incident protons will generally exceed these values. The energy of the ions and neutral particles in the atmosphere is on the order of 7 to 14 ev. if the thermal motion of these particles is neglected. The yield for energies of this level has been measured at 5×10^{-5} atoms per particle for chromium erosion.

The question of ionization or change in dielectric properties due to lattice defects by the incident charged particles is the most difficult of the effects to ascertain. The basic mechanism of importance in ionization is the creation of free electrons for bound excited states (excitons) which could propagate through the medium, giving it some of the properties of a conductor. Since the reflective characteristics of a medium are determined by dielectric properties, a significant amount of ionization could conceivably alter a material. No directly applicable experimental evidence on this subject has been found.

In summary, surface erosion of the surface may be sufficient to influence the optical properties of a mirror. Even with pessimistic assumptions (e.g., high sputtering yields), it appears that optical surfaces can last for several years using coatings several microns in thickness in those regions of most danger, i.e., low satellite orbits and interplanetary missions beyond 6 earth radii from the surface. Between these regions where dense atmospheric particles and high energy solar "winds" occur, it appears that the erosion hazard becomes small, and a zone of relative safety extends from altitudes of perhaps 500 to 24,000 miles. These conclusions must be regarded as preliminary until more definitive data from space probe and satellite instrumentation is obtained.

The performance of solid state electronic components will be degraded if exposed to the proton and electron bombardment of the Van Allen belt. For example, it is estimated that a photovoltaic cell will function only for a few days in the most intense proton bombardment of the inner Van Allen belt due to destruction of the regular crystal lattice structure. The estimated degradation is discussed in detail in Volume V, Section A

4.0 METEOROIDS

Any estimate of meteoroid effects on a space structure depends on data of two general categories; the frequency with which a surface will be struck by a particle with a given size, velocity, direction and composition; and the destructive effects of that particle on the particular surface used. No direct experimental evidence is as yet available in either of these areas and estimates of structural deterioration in the space environment rely on extrapolations and theoretical arguments.

The meteoroid particles of most interest are of relatively small dimensions and are unobservable by visual, photographic, or radar techniques. Any estimate of the numbers, velocities, masses, and other fundamental characteristics must be extrapolated beyond the range of direct observation. Such programs as the Harvard Photographic Meteor Program have led to precision results in terms of visible meteoric velocities, luminous intensities, decelerations and trajectories. Recent radar observations have added information concerning atmospheric ionization and seasonal distribution of meteors, and has extended the range for observation to particles as small as 10^{-3} m.

4.1 Incidence

On the basis of the Harvard Photographic Meteor Program, a meteor of visual magnitude 0 was determined to have a mass on the order of 25 grams. Theoretical arguments indicate a mass decrease by a factor of 2.514 per visual magnitude step or magnitude $2.5\log_{10}(m_0/m)$. The total mass of meteoroids contributed by each magnitude step is roughly a constant in the visual range (from zero to fifth magnitude) and is assumed to be constant in the smaller particle range. The number of particles of a given mass impinging on the earth per day is then given by:

$$N_{earth} = \frac{5.83 \times 10^{7}}{m} \qquad (1)$$

where N_{earth} = Number of particles/earth surface-day

m = Particle mass (gr.)

This formula is based on the data presented by Whipple and is considered by authorities to be the best numerical estimate at this time. Incidence can be predicted to within I 20°/o for meteors of visual magnitude from zero to the 5th magnitude (except for rare heavy showers). The uncertainty in the incidence of meteoroids from the fifth to the 8th magnitude is perhaps 30°/o, as determined by radar measurement. The incidence of smaller particles can only be extrapolated until adequate satellite measurements are made. Equation (1) is depicted in Figure 8, and is plotted as a function of N, the number of particles of mass greater than m grams incident on a flat plate of 1 m^2 per sec. The variation in N resulting from a variation in the assumed mass of a zero magnitude meteor is also shown. Recent satellite data has indicated a particle frequency dependence closer to $m^{-1.09}$.

(Explorer I, Vanguard III) as follows:

$$N = 10^{-12} m^{-10/9} \quad (m^2 sec) \qquad (2)$$

where N = number of particles incident on flat plate in satellite orbit.

This formula is graphically depicted in Figure I-B-8.

It should be noted that the satellite data was taken in the vicinity of the earth so that the satellite is shielded by the meteoroid flux in one direction. Therefore, the flux should about double as one travels a few earth radii into space. It should also be noted that data from satellites and space probes disagrees, as indicated by the data point for Pioneer I. This disagreement could easily result from the low number of impacts from which

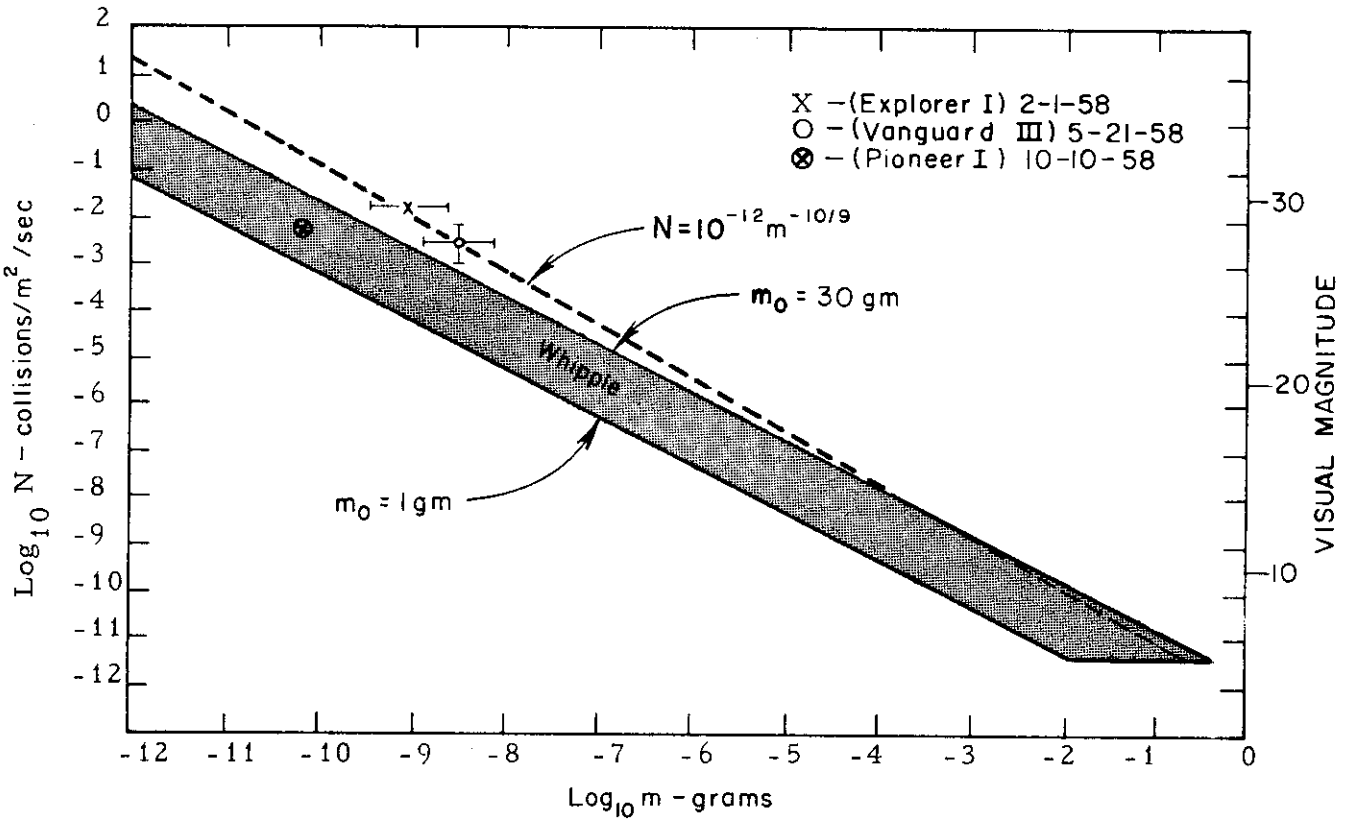

FIGURE I-B-8 METEOROID FLUX VERSUS MASS NEAR EARTH

estimates are derived. The incidence of meteoroids as a function of position in the solar system is indicated both by the statistical data on the orbits of meteor swarms and by the satellite data. The latter indicated that the incidence of meteors on the side of the earth toward its direction of orbital motion was over four times that for the reverse side. Both factors indicate that there should be little difference in the incidence rate of meteoroids in the vicinity of the earth's orbit, but that the frequency might increase by conceivably a factor of 10 near the orbit of Mars. On the other hand, incidence should not change substantially in regions approaching the orbit of Venus. The influence of the earth's gravitational field has small effect.

4.2 Mass Density and Velocity

From his work on many Harvard photographic meteors, Dr. L. G. Jacchia finds as a constant for determination of mass and density among photographic meteors the following relationship applying at visual magnitude zero:

$$C_d \quad \frac{\text{Area}}{\text{Mass}} = 9.1 \text{ (cgs)} \tag{2}$$

where C_d is the standard drag coefficient, Area is the frontal area of the meteoroid, Mass is the total mass of the meteoroid, the quantity derives from the drag equation:

$$\frac{dv}{dt} = \frac{-C_d}{2} \frac{\text{Area}}{\text{Mass}} \rho v^2 . \tag{3}$$

The velocity v and deceleration dv/dt were measured as mean values for many meteors while the air density ρ was adopted from the best available 90 km; the equation applies for $v = 30$ km/sec.

The constant of the first equation can be transformed into a function of meteoritic density, ρ_m, and a shape factor, A (dimensionless). For a sphere A = 1.209, for a randomly oriented brick of dimensions 2 x 3 x 6, A = 1.66, for a brick of dimensions 1 x 6 x 6, A = 2.04, and for a cube, A = 1.50.

Hence, the first equation can be rewritten:

$$\frac{C_d A}{m^{1/3} \rho_m^{2/2}} = 9.1 \text{ (cgs)}. \qquad (4)$$

This equation becomes finally:

$$m(O^m \text{ Visual}) = \frac{(C_d A)^3}{\rho_m^2} \times 1.33 \times 10^{-3} \text{ (cgs)}. \qquad (5)$$

If we choose, for example, $C_d = 2$, $A = 1.66$, and $\rho_m = 0.05$ gm/cm^3, we find that $m\,(O^m \text{ visual}) = 19.5$ gm.

The determination of the mass of a meteor of a given photographic magnitude depends on the luminous efficiency, that is, the fraction of the kinetic energy of the meteor that is converted into visible light. It is believed that this factor is about 0.001%, but the uncertainty factor may still be two orders of magnitude. A similar uncertainty is associated with the ionization efficiency in reducing radar data. The mass of a zero-magnitude meteor will probably run somewhere between 2 and 20 gm although the range may be as great as 1 to 30 gm. The result of this uncertainty in predicting the incidence of smaller particles is shown by the shaded zone of Figure 8.

The average density of photographic meteors is probably around 0.05 g/cm^3. There apparently is a wide variation in

meteoroid density, the majority having densities within a factor of two to four of the average, although occasional meteoroids run perhaps a factor of 10 less dense, and extremely rare fragments may be a factor of 100 more or less dense than the mean.

Two sets of photographic plates are available which permit the determination of the meteoroid mass per unit of cross-sectional area, but the data from the second of these two plates have not yet been reduced. If a meteoroid density of 0.05 g/cm^3 is assumed, the plates indicate that the luminous efficiency is 0.002% at 40 km/sec. In any event, the average mass per unit area for meteors having magnitude of one is probably known within a factor of two or better.

This may entail an error in penetration estimates substantially less than might appear to follow from the uncertainty in meteoroid density because hypervelocity projectile measurements indicate that the penetration will vary inversely as the 0.3 to 0.6 power of the density.

The value of .05 g/cm^2 depends upon physical arguments from photographic meteor data and from measurements of the momentum imparted to the atmosphere by a meteoroid. Additional evidence results from the phenomena of irregular flares and breaking-up of meteors at low atmospheric pressures. Meteors having a common origin from a given comet tend statistically to be more alike than those from different comets although the variations are still quite pronounced.

Less than 10 percent of all visible meteors are estimated to be hard, high density materials varying in composition from stone (2.8 grams/cm^3) to iron (8 grams/cm^3). The proportion of stony to iron meteors is about 10 to 1 and a current working hypothesis is that these particles are of asteroidal origin and consequently are concentrated in the region between Mars and Jupiter.

Nothing is known about the density or chemical composition of the smaller particles in the solar system although they are presumably cometary in origin. The densities are very probably higher than those believed to occur for the visible meteors with densities approaching that of stone and iron. The cross-over point where high density particles become as numerous as low density particles is probably on the order of 5 to 10 visual magnitude.

The velocity range of a particle striking the earth is from 11.3 to 73 kilometers per second, an average velocity of 28 kilometers per second with respect to the earth has been observed for photographic meteors. This average will decrease with particle size, with an average value of 15 kilometers per second being used in calculations for smaller particles. A satellite velocity relative to the earth of roughly 8 to 9 km/sec would extend this range (2 to 81 km/sec).

Small particles would be strongly influenced by the Polyting-Robertson effect. The effect of absorption and subsequent emission of solar radiation by an isolated particle in the solar system will

introduce a resisting force proportional to the velocity of the particle, producing a slow circular decrease in the size of the particle orbit until a particle eventually falls into the sun. Under the Polyting-Robertson deceleration, the dust eccentricity decreases more rapidly than dust perihelia. By the time interplanetary dust particles reach aphelia on the order of an astronomical unit or less, the motion is predominantly circular. The average particle velocity undoubtedly falls off for smaller meteoroids due to the increased relativistic aberration from the Polyting-Robertson effect.

Extrapolation of observable meteor data would infer high concentrations of small particles. Particles sufficiently small, however, experience a greater repulsive force due to solar radiation pressure than an attractive force due to gravitation. For non-reflecting black spheres, the minimum particle radius a is given by:

$$a \geq \frac{0.6}{\rho} \text{ microns} \tag{6}$$

where ρ = specific gravity of particle

Smaller particles would be blown out of the solar system. Whipple has also suggested that high energy protons from the sun may have an effect on both this purely electromagnetic pressure result and the Polyting-Robertson effect. Equation (3) indicates that low density particles with radii less than 12 microns will not be encountered and that high density particles of radii less than 1 micron and mass less than 3×10^{-11} (magnitude = 30) will not be encountered. For the purpose of calculations in this text, the upper estimated limited

of average impacts/day (m_o = 30 gr).

4.3 Penetration

Authorities generally agree that Bjork's theoretical model of hypervelocity impact and penetration has most validity at present. Bjork programmed on a digital computer the case where a cylinder impacts normally against an infinite plane of the same material. The cylinder's height equalled its diameter. At impact a shock wave spread from the point of impact through the material. The material left behind the shock wave was compressed very much in excess of the ultimate yield stress and the behavior of the material was expressed by the hydrodynamic equations for compressible, inviscid, adiabatic flow. This theory is in opposition to many previous assumptions where it was assumed that at impact velocities above the velocity of sound in the target (about 5 km/sec in steel), the energy was unable to escape as it cannot propagate with velocity greater than that of sound, resulting in an explosion. Bjork showed that this supposition was incorrect and the velocity can reach speeds far in excess of the velocity of sound in the target. The resulting material flow created craters of roughly a hemispherical nature.

Bjork's results are summarized by the equations

$$\begin{aligned} &\text{Al on Al:} && P = 1.09\,(mv)^{1/3} \\ &\text{Fe on Fe:} && P = .606\,(mv)^{1/3} \end{aligned} \qquad (7)$$

where P = depth of penetration in cm.

m = projectile mass in grams

v = impact velocity in km/sec.

The calculated craters are hemispherical with radium ρ. In the range of pressures developed in the impact, iron and steel behave

identically. The calculations were made for thick targets but enough information was obtained to deduce that if a projectile penetrates a depth, ρ, in a thick target, it will penetrate a sheet of the same material which is 1.5 ρ thick.

Experimentation on penetration has been limited to low speeds with particle velocities up to about 15 km/sec being attained with small particles on the order of to 200 microns in diameter. Differences in experimental results can be attributed to the different target and particle materials used, particle shapes, velocities, and other variations.

The compressibility of the projectile and target material are obviously of importance as described by Bjork. In addition, the densities of both materials are important in that they determine, in part, the shape and intensity of the stress wave developed during the initial stages of impact. Wave propagation rates in both projectile and target materials are clearly important for the same reason; they determine the extent to which the energy of the system can be distributed throughout the volume of the two bodies. And, lastly, the strengths of the materials are important, especially that of the target material. The tremendously high pressures and strain rates existing during the initial impact do not prevail throughout the process; during the later stages of crater formation, the pressure and velocity will both have been reduced to such a degree that ordinary material strengths will become important. It should be kept in mind that the strength characteristics that are important in phenomena of the sort under consideration are not the usual static yield or ultimate

tensile strengths but are the strengths prevailing under high rates of loading or high strain rate. It has been found, under conditions similar to those existing in hypervelocity impact, that yield strengths as much as ten times the static values can be observed.

Figure I-B-9 shows a typical plot of the ratio of crater depth to crater diameter as a function of the impact velocity, for steel projectiles fired into lead targets (Eichelberger). At very low impact velocities, the ratio of depth to diameter increases with increasing velocity until cavitation begins to play an important role. Thereafter the ratio decreases systematically until it reaches a value 0.5, corresponding to a hemispherical crater, and thereafter remains constant. For the particular combination of projectile and target material used, the hemispherical crater was first observed at an impact velocity approximately equal to the velocity of a plastic wave in the target material. This, however, is only coincidental since the limiting velocity depends upon the projectile material as well as the target material. The general form of the curve shown is typical of cases in which hard projectiles are fired into soft target materials. If the materials are identical or if the projectile material is softer than the target material, the ratio of depth to diameter tends to increase monatonically from small values to the value 0.5. In all cases investigated to date, however, when sufficiently high velocities are attained (i.e., less than about 10 km/sec) the ratio is equal to 0.5.

In Figure I-B-10 are shown typical plots of crater depth as a function of impact velocity as presented by Eichelberger.

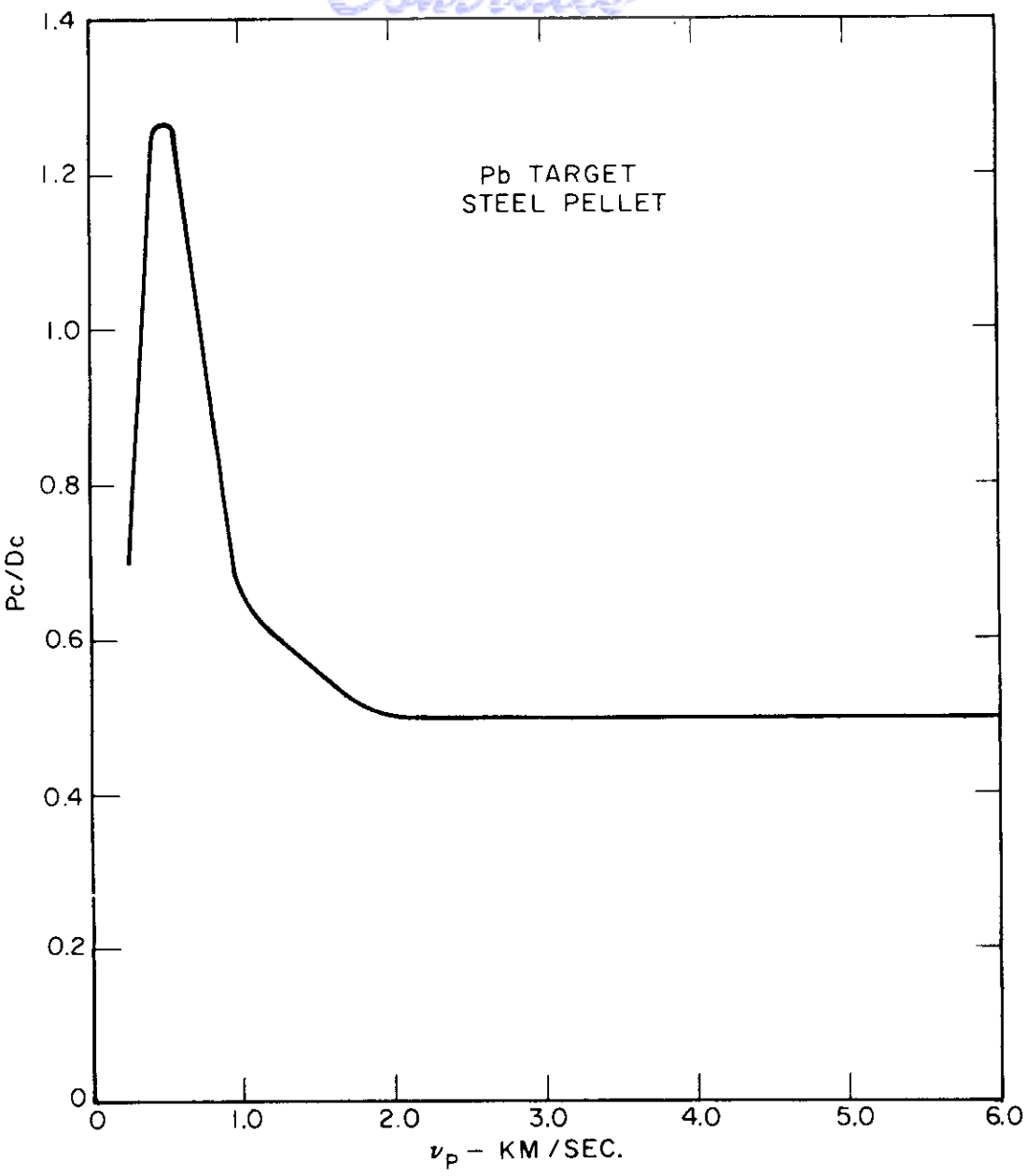

FIGURE I-B-9 PENETRATION VS. IMPACT VELOCITY

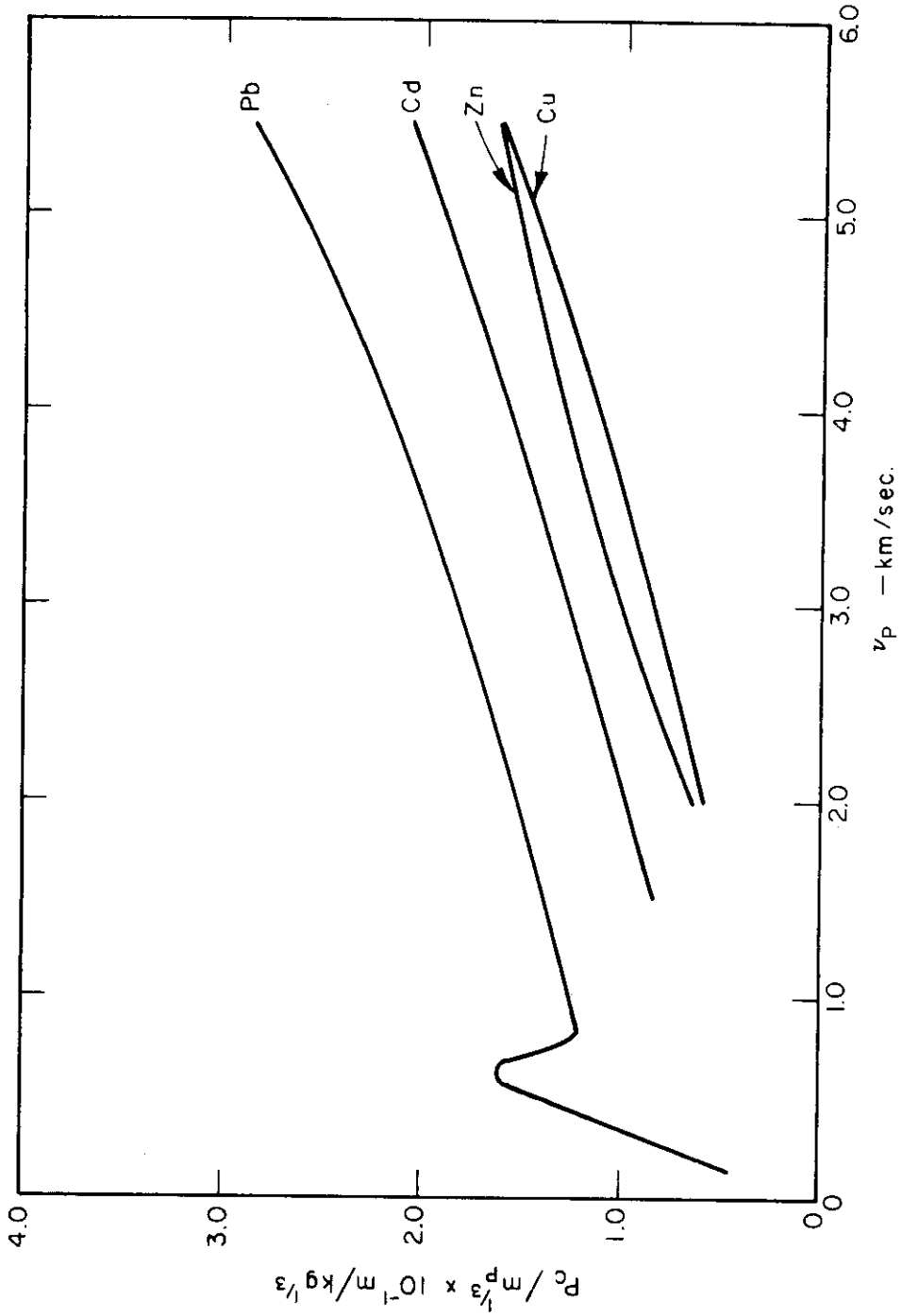

FIGURE I-B-10 PENETRATION VS. IMPACT VELOCITY FOR FOUR TARGET MATERIALS

In this case the crater depth has been normalized by dividing by the cube root of projectile mass, in accordance with established scaling laws. Results with lead, cadmium, zinc, and copper targets are shown. Steel projectiles weighing 1/10 to 10 grams were used. Those with lead targets cover a much wider velocity range and show the peculiar behavior at relatively low impact velocity. At very low velocity the depth of penetration increases rapidly with increasing velocity until a point is reached at which severe deformation and perhaps shattering of the projectile occur. Thereafter, for a short period, the depth of penetration actually decreases with increasing impact velocity until a condition is reached wherein cavitation begins to play an important role. Thereafter, the depth of the crater increases smoothly and monatonically within increasing impact velocity. It should be noted that the rate at which the crater increases with increasing velocity is approximately the same for all four target materials represented. The determinations are not sufficiently complete at the present stage of the experiment to permit description by means of empirical formulae nor can it be stated with certainty that the systematic variations shown for the velocity range covered will persist indefinitely into the hypervelocity regime. When particles approach the grain size of the material of the target, it has been found that wide variations in the ratio of crater depth to diameter occur. The anistropies in the strength characteristics of the crystals become important, and crater depths are much greater than predicted. Experimental data has indicated that at velocities where hemispherical cratering begins (2 - 10 km/sec), the angle of incidence of the particle will not affect crater size or shape up to oblique angles

on the order of 70°. Problem areas which should be investigated in the future include the fragmentation which might occur depending on the crystal structure, heat treatment and other properties of the material; spalling and other effects when surface coatings are used, and other problems.

The impact data so far taken in laboratories indicates that among particles of the same mass and velocity, the one of greatest density gives the largest penetration. One definitive set of experiments has been performed by Summers and Charters. They performed a series of tests at 7,000 ft/sec (2.13 km/sec) keeping the projectile mass constant and using the same target material. Using spherical projectiles of various metals, they covered the density range of 1.5 to 17.2 gm/cm^2. For each of the target materials used, they found their results could be correlated with the density ratio between projectile and target material; for example:

$$\begin{aligned} &\text{copper targets:} && p \sim (\rho_p/\rho_t)^{.6} \\ &\text{lead targets:} && p \sim (\rho_p/\rho_t)^{.3} \end{aligned} \qquad (8)$$

where ρ_p and ρ_t are the projectile and target densities, respectively.

It seems too optimistic to expect that the same relation would hold at velocities several times higher than that used in obtaining the empirical fit, or at densities many times lower. But it does seem plausible to expect that the general trend would be the same, so that overestimating the projectile density results in overestimating the penetration. On this basis, it is conservative to use Bjork's results of Equation (7) directly to predict the penetration. This equation will

almost certainly overestimate the meteoroid damage considerably in the photographic meteor range, where there is a good indication that the meteors have a low density. On the other hand, the meteors of such great mass are very infrequent, and it will be seen that for all practical purposes, their presence may be neglected in designing something like a radiator required to operate in space for a year with a 90 percent probability of suffering no damage at all from meteoroids.

It is reasonable to expect that the smaller meteoroids will not have the lacy, porous structure needed to give a specific gravity of .05, but that their density will increase as one goes down the mass scale, eventually approaching the specific gravity of stone, the basic component, as very small sizes are reached. No evidence exists to indicate what the functional dependence of density upon mass will be. The specific gravities of stone, aluminum, and steel are 2.8, 2.7, and 8.0, respectively. Thus, for stony density particles, Eq. (7) may be expected to give a good approximation for meteoroids vs. aluminum, but to still overestimate slightly the effects of meteoroids vs. steel.

4.4 Penetrating Flux

Combining Equations (2) and (7), one obtains for the penetrating flux

$$\psi = 10^{-12} t^{-10/3} K^{10/3} v^{10/9} \qquad (9)$$

where ψ is the number of penetrations per square meter per second of a target 5 cm thick, if the meteoroid velocity is v km/sec.

Aluminum targets: $K = 1.5\ (1.09) = 1.64;\ K^{10/3} = 5.20$

Steel targets: $K = 1.5\ (.606) = .908;\ K^{10/3} = .725$

The estimate of ψ as a function of t for aluminum and steel is summarized in Figure I-B-11 and Table I-B-4. To compute the visual magnitude, an m_o of 25 gm was used. Whipple's estimate of the average meteoroid velocity as a function of the mass was used and varies from 28 km/sec at M = 0 to 15 km/sec at $M \geq 20$. Figure I-B-11 also shows the effect of assuming the incident meteoroids are of low density material with $\rho = .05$ g/cc.

The effectiveness of the optical surface of a solar concentrator and surface coatings of various types used for radiator and absorber structures will be affected by the average depth of surface coating destroyed by meteoroids. The total volume of surface destroyed by all penetrating particles can be determined by assuming a hemispherical crater and integrating the product of particle number and hole diameter over the range of particles encountered. The surface area destroyed can be determined in a similar fashion. Using the most pessimistic assumptions the total surface area destruction is much less than 1 percent of the total.

TABLE I-B-4

ESTIMATE OF PENETRATING FLUX

Visual Magnitude	Mass gm	Velocity km/sec	Aluminum Thickness cm	Steel Thickness cm	Penetrating Flux Penetrations m^2-sec
0	25.0	28.0	14.5	8.06	2.80×10^{-14}
1	9.95	28.0	10.7	5.93	7.79×10^{-14}
2	3.96	28.0	7.85	4.36	2.17×10^{-13}
3	1.58	28.0	5.78	3.21	6.02×10^{-13}
4	0.628	28.0	4.25	2.36	1.68×10^{-12}
5	0.250	28.0	3.13	1.74	4.67×10^{-12}
6	9.95×10^{-2}	28.0	2.30	1.28	1.30×10^{-11}
7	3.96×10^{-2}	28.0	1.69	0.940	3.62×10^{-11}
8	1.58×10^{-2}	27.0	1.23	0.684	1.00×10^{-10}
9	6.28×10^{-3}	26.0	0.894	0.496	2.80×10^{-10}
10	2.50×10^{-3}	25.0	0.649	0.360	7.78×10^{-10}
11	9.95×10^{-4}	24.0	0.471	0.261	2.17×10^{-9}
12	3.96×10^{-4}	23.0	0.341	0.190	6.03×10^{-9}
13	1.58×10^{-4}	22.0	0.248	0.138	1.67×10^{-8}
14	6.28×10^{-5}	21.0	0.179	9.96×10^{-2}	4.67×10^{-8}
15	2.50×10^{-5}	20.0	0.130	7.21×10^{-2}	1.30×10^{-7}
16	9.95×10^{-6}	19.0	9.28×10^{-2}	5.21×10^{-2}	3.61×10^{-7}
17	3.96×10^{-6}	18.0	6.78×10^{-2}	3.76×10^{-2}	1.01×10^{-6}
18	1.58×10^{-6}	17.0	4.90×10^{-2}	2.72×10^{-2}	2.79×10^{-6}
19	6.28×10^{-7}	16.0	3.53×10^{-2}	1.96×10^{-2}	7.78×10^{-6}
20	2.50×10^{-7}	15.0	2.54×10^{-2}	1.41×10^{-2}	2.17×10^{-5}
21	9.95×10^{-8}	15.0	1.87×10^{-2}	1.04×10^{-2}	6.03×10^{-5}
22	3.96×10^{-8}	15.0	1.37×10^{-2}	7.63×10^{-3}	1.68×10^{-4}
23	1.58×10^{-8}	15.0	1.01×10^{-2}	5.62×10^{-3}	4.66×10^{-4}
24	6.28×10^{-9}	15.0	7.44×10^{-3}	4.13×10^{-3}	1.30×10^{-3}
25	2.50×10^{-9}	15.0	5.47×10^{-3}	3.04×10^{-3}	3.61×10^{-3}
26	9.95×10^{-10}	15.0	4.03×10^{-3}	2.24×10^{-3}	1.01×10^{-2}
27	3.96×10^{-10}	15.0	2.96×10^{-3}	1.64×10^{-3}	2.80×10^{-2}
28	1.58×10^{-10}	15.0	2.18×10^{-3}	1.21×10^{-3}	7.77×10^{-2}
29	6.28×10^{-11}	15.0	1.60×10^{-3}	8.90×10^{-4}	0.217
30	2.50×10^{-11}	15.0	1.18×10^{-3}	6.55×10^{-4}	0.603
31	9.95×10^{-12}	15.0	7.68×10^{-4}	4.82×10^{-4}	1.68

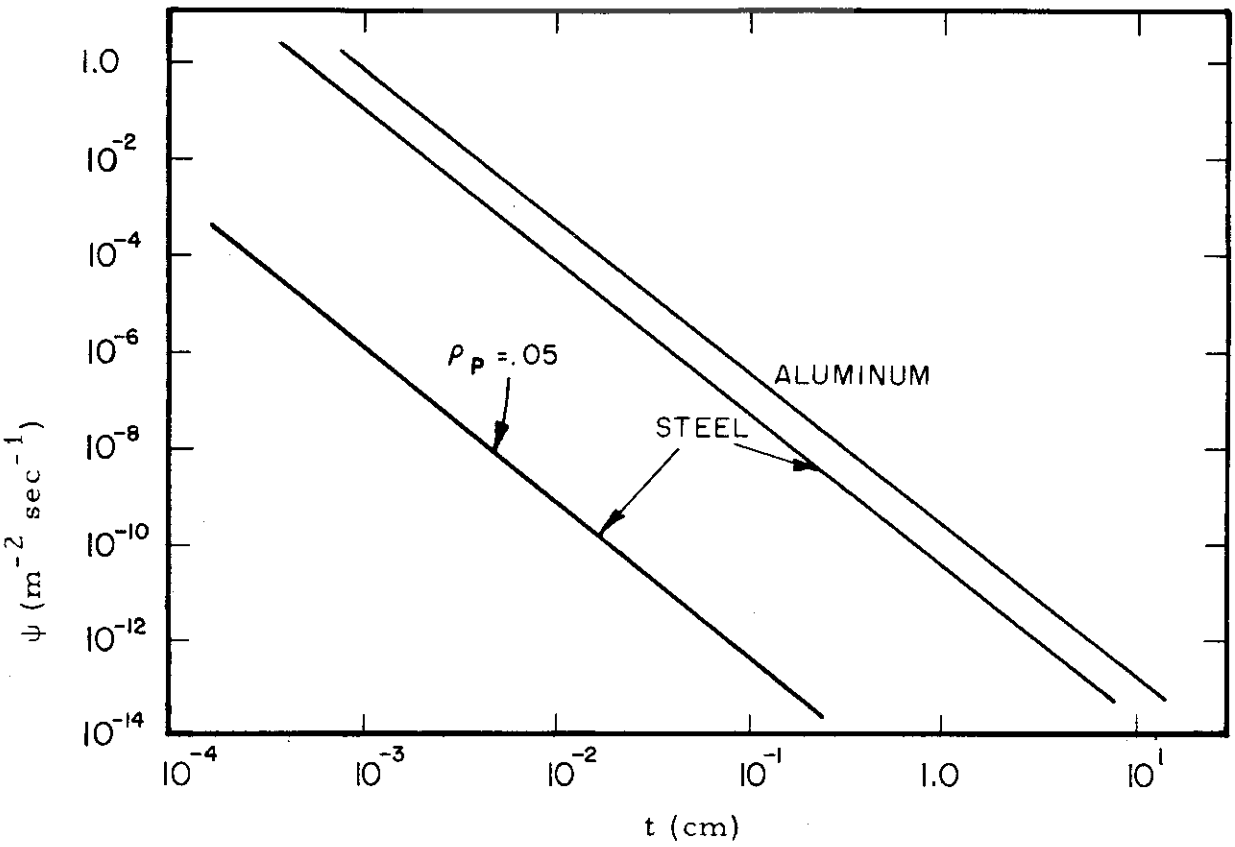

FIGURE I-B-11 PENETRATING METEOROID FLUX NEAR EARTH VERSUS SKIN THICKNESS

REFERENCE LIST

This list partially summarizes the reference material dealing with the space environment and its effects. The documents listed here are of a general survey nature in several cases representing a collection of papers, suitable for preliminary investigation.

1. Gayley, J.C., Kellogg, W.N., Vestine, E.H., "Space Vehicle Environment". Journal of the Aero/Space Sciences, Vol. 26, No. 12, Dec. 1959

2. "Materials in Space Environment", Proceedings of the Fifth Sagamore Ordnance Materials Research Conference, Sept. 16-19, 1958, ASTIA No. AD205 880

3. 1960 Proceedings of the Institute of Environmental Sciences, April 6-8, 1960, Los Angeles, Calif.

4. First Symposium "Surface Effects on Spacecraft Materials", 1 October 1959, Lockheed Missiles and Space Division, LMSD-288044

5. Johnson, Francis S., "The Composition of Outer Space", Astronautics, April, 1960

6. Reiffel, S., "Structural Damage and Other Effects of Solar Plasmas", Journal of the ARS, Vol. 30, No. 3, March 1960

7. Jaffe, L.D., Jet Propulsion Laboratory Memos

   "Plastics in Space Environment" 4-13-60
   "Evaporation of Metals and Semiconductors in Space Environment" 7-23-59
   "Sputtering and Meteroid Damage to Materials in Space" 1-25-60

8. 1960 Proceedings of the National Aeronautical Electronics Conference, May 2-4, 1960 - Session on Interplanetary Environment

9. Whipple, F.L., "The Meteoric Risk to Space Vehicles", Vistas in Astronautics, Pergamon Press

10. Manning, E. and Dubin, M., Satellite Micro Meteorite Data, National Academy of Sciences, IGY Satellite Series No. 3, May 1, 1958

11. Bjork, R.L., "Effects of a Meteroid Impact on Steel and Aluminum in Space", Rand Document P-1662, December 1958

REFERENCE LIST (continued)

12. Conference on the Meteoroid Hazard to Space Power Plants, December 1-2, 1959, Washington, D.C. - Chairman, G.M. Anderson, A.P. Fraas

13. Whipple, Fred L., "Solid Particles in the Solar System", Journal of Geophysical Research, Vol. 64, No. 11, November 1959

14. Dubin, Maurice, "The Meteoric Environment from Direct Measurements" and "Meteoric Dust Measured from Explorer I"

15. Van Allen, J.A., and Frank, Louis A., "Radiation Around the Earth to a Radial Distance of 107,400 km", Nature, Vol. 183, February 14, 1959

16. Babinsky, A.D., Del Duca, M.G., Bond, A.F., "The Radiation Problem in Low Thrust Space Travel", ARS Paper No. 989-54

17. Wood, G.P., Carter, A.F., "Predicted Characteristics of an Inflatable Aluminized-Plastic Spherical Earth Satellite with Regard to Temperature, Visibility, Reflection of Radar Waves, and Protection from Ultraviolet Radiation"

ENERGY CONVERSION SYSTEMS REFERENCE HANDBOOK

Volume I - General System Considerations

Section C

RELIABILITY CONSIDERATIONS IN POWER SYSTEM DESIGN

W. R. Menetrey
Energy Research Division
ELECTRO-OPTICAL SYSTEMS, INC.

Manuscript released by the author
September 1960 for publication in this
Energy Conversion Systems Reference Handbook

I-C RELIABILITY CONSIDERATIONS IN POWER SYSTEM DESIGN

C O N T E N T S
and
I L L U S T R A T I O N S

Figures

I-C RELIABILITY CONSIDERATIONS IN POWER SYSTEM DESIGN

Power systems for space application will incorporate components intended for periodic or constant use over long periods of time. The reliability of components of this type is usually characterized by the measurement of a failure rate of a number of samples in actual equipment use or while testing equipment under simulated conditions. The failure rate is obtained by dividing the total operating hours of a number of components during a given short time interval into the failures during that interval. These components must be of the same model with common usage conditions and a common criteria of failure.

1.0 EQUIPMENT CHARACTERISTICS

Equipment can be generally described by the failure rate curve of Figure I-C-1. As shown, a period of high but decreasing failure rate occurs in the first few hours of operating time due to marginal parts and material and other causes which can be generally eliminated by careful inspection and fabrication. It is important that this period be determined and removed prior to using components in order to enter the region of low failure rate.

Following the early failure period, an extended period of relatively constant failure rate occurs. Here, failures occur randomly and chance of failure is independent of age. Causes of failure of major importance during this period will include the following:

a. The catastrophic destruction of component by meteoroid bombardment, sudden malfunction, etc.

b. Random internal failures due to unavoidable human error, random occurrence of stresses, and other uncontrolled variations.

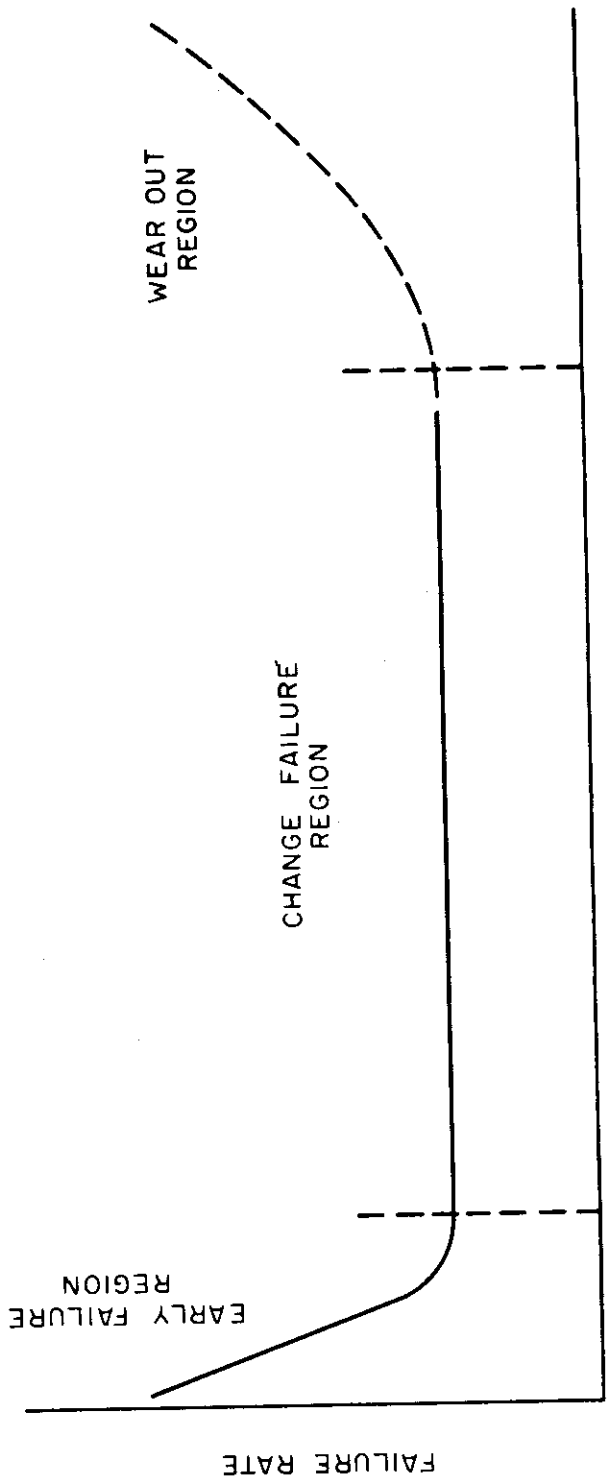

FIGURE I-C-1 CHARACTERISTIC FAILURE RATES OF EQUIPMENT

The equipment will finally enter a wear-out region with an increasing failure rate. Major causes of wear-out will include such items as:

a. The gradual deterioration of materials due to high temperature, high pressure, and other maximum stress conditions.

b. The erosion of surfaces exposed to the space environment.

c. The deterioration of components sensitive to high energy electromagnetic and corpuscular radiation.

The assumption of constant failure rate is a special case where the absence of any significant fatigue or wear-out effects is assumed valid for a long period of operation. This assumption is a mathematically convenient approximation which does not apply to all equipment. Using this approximation, the reliability of a component is expressed by

$$R = \exp\left[\frac{-t}{\theta}\right]$$

where R = probability of successful operation up to time, t.

θ = mean time to failure for constant failure rate.

In the general case, a variation of the Wiebull distribution (Flehinger and Lewis) has been found particularly useful for failures where fatigue or wear-out is significant. It may be written as

$$R = 1 - \exp\left[-\frac{t}{\theta_r} - \left(\frac{t}{\theta_t}\right)^m\right]$$

where m = an integer.

For example, analysis of field data concerning aircraft generators and starters has indicated values of m = 2, and θ_t / θ_r from .5 to 2.5 to be appropriate depending on specific design*. The mean time to failure is less than that predicted for the constant rate of failure case. For the case where m = 2, some values of this ratio are given below as a function of the parameter θ_t / θ_r.

*Duane, J.T., and Yeager L.J., "Reliability Analysis for Aircraft Generators", AIEE Proceedings, January 1960.

θ_t/θ_r	TMF/θ
0	1.0
.5	.7
1	.55
2	.37
4	.22

Citing this example, it would be foolish to apply a constant failure rate criterion to each component without sufficient experimental field and/or simulated data. The difficulty of gathering sufficient data is illustrated by assuming a constant failure rate and listing some ratios of mean time to failure to mission length to insure a given reliability.

R	θ/t
.9	9.5
.95	19.5
.99	100
.995	200

Thus, the mean time to failure for a component must be demonstrated to be 195,000 hours to expect 95 percent reliability for a 10,000 hour mission (1 year = 8760 hours). Conversely, a component with θ = 10,000 hours will have a 36.8 percent (1/e) probability of completing a 10,000 hour mission.

2.0 STATISTICAL TESTS

Reliability estimates of component performance will rely on samples tested on the ground. Enough samples must be provided for high confidence.

Several sampling plans for determining the mean time to failure of a system and its components where times to failure are exponentially distributed, have been developed and are well known.

In practice, the number of observations required to obtain significant statistical data can be substantially reduced when the observations are made one after another or in small groups and various sequential analysis techniques are applied. The experiment is stopped as soon as there is sufficient evidence to indicate that one or the other of two alternative hypothesis is accepted. Tests of this nature unfortunately cannot be used on many components due to the lack of knowledge regarding the extrapolation from tests conducted over a few months to operation over years.

Briefly; sequential analysis involves the following steps:

a. Assume a statistical distribution of failures like the binomial or Poisson. Distribution free procedures may be employed in sequential analysis to obtain more rigorous decisions, but take more time.

b. Select two values of reliability, failure rates, or mean time between failures. One value should be at a level for satisfactory acceptance of the equipment and the other level that is intolerable; i.e., requires rejection of the equipment. The farther apart these values are selected, the more reliable will be the statistical decision as to which value is most likely to be correct.

c. Decide what fraction of the time decisions to accept must be correct, $1 - a$; and what fraction of the time reject decisions must be correct, $1 - \beta$. The resulting sequential statistical

analysis yields a test plan which may be presented graphically, as shown in Figure I-C-2.

According to Figure I-C-2, it is possible for a particular set of test results to remain in the no-decision region indefinitely. Wald* has proven that the probability of arriving at a decision is unity if given infinite time, but this is not very gratifying. A more satisfactory solution is to truncate the testing after a certain amount of environmental operation and/or a certain number of failures. Wald* has developed the relation for the reduction in confidence of accept or reject decisions for truncated test plans.

The use of sequential analysis techniques results in large savings in terms of the number of trials required to specify equipment reliability. Another advantage of sequential methods is the capability of following progress during system evolution as indicated by the test data. This allows interim reliability estimation and determination of the effectiveness of component improvements.

One difficulty with using normal sequential analysis in a development program is that the low reliability of early tests may indicate immediately that the equipment was unsatisfactory. In normal inspection procedures this would mean rejection. However, a development program is intended to improve inadequate equipment rather than reject it. An analysis procedure is required to show whether current equipment is satisfactory without regard to early test history.

*Wald, A. "Sequential Analysis," John Wiley and Sons, Inc., New York, 1947.

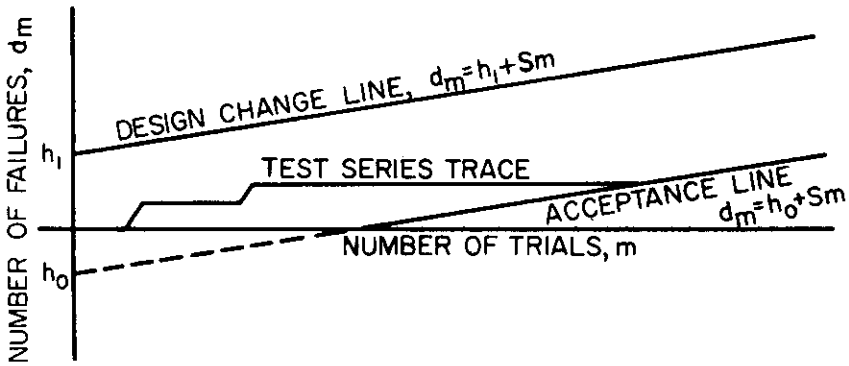

$$h_o = \text{Acceptance Line Intercept} = \frac{\text{Log}\,\frac{\beta}{1-\alpha}}{\text{Log}\,\frac{p_1}{p_o} - \text{Log}\,\frac{1-p_1}{1-p_o}}$$

$$h_1 = \text{Design Change Line Intercept} = \frac{\text{Log}\,\frac{1-\beta}{\alpha}}{\text{Log}\,\frac{p_1}{p_o} - \text{Log}\,\frac{1-p_1}{1-p_o}}$$

$$S = \text{Slope of Lines} = \frac{\text{Log}\,\frac{1-p_o}{1-p_1}}{\text{Log}\,\frac{p_1}{p_o} - \text{Log}\,\frac{1-p_1}{1-p_o}}$$

Acceptance indicates confidence $1 - \beta$ that reliability is at least $1 - p_1$ (lower reliability limit)

Design change requirement indicates confidence $1 - \alpha$ that reliability is less than $1 - p_o$ (upper reliability limit)

Figure I-C-2 SEQUENTIAL ANALYSIS FORMULAE

Recently, a solution was proposed to the problem of statistical evaluation of tests with changing reliability, i.e., to reverse the order in which tests are considered as compared with the usual sequential analysis. With this reversed sequential analysis, the most recent test result is plotted at the origin of the graphical test plan chart and each earlier test is plotted further from the origin. Early test results are continuously displaced from later consideration and have a reduced influence on later decisions. This procedure, in effect, compensates for equipment deterioration during a series of tests. The limited number of tests available for most practical programs, however, prevents the acceptance of seriously deficient equipment. Further investigation into the consequences of reversed sequential analysis is required.

3.0 REDUNDANCY

In general, n components will be grouped in a unit of series and each system will contain m number of units connected in parallel. If one unit malfunctions, system performance will deteriorate by a factor of n - 1.

Two typical design questions are:

a. What is the optimum compromise between the desirability of maximizing m for reliability and decreasing m for lighter weight.

b. How many extra units must be provided to insure a 95.0 percent reliability that the system will provide a given power level during the mission.

For a unit with n components in series, the relationship between component reliability and unit reliability, is simply

$$R_{unit} = r^n$$

where

R = individual component reliability.

This equation is plotted in Figure I-C-3 for different values of n and R, assuming R is equal for each component.

Assuming components with a reliability of about 99 percent, Figure I-C-3 shows that 95 percent unit reliability will be attained with 5 components in series, and that 10 components in series would result in about 90 percent unit reliability.

The reliability of a complex system can be generally increased by adding redundant components. Two methods of incorporating redundancy are shown in Figure I-C-4. It can be seen that for the same number of components the series parallel mode is inherently more reliable than the parallel mode. The increase in reliability is illustrated in Figure I-C-5.

For example, assume that

θ = 10,000 hr

t = 10,000 hr

n = 1

consequently r = .368

then if the desired value of over-all reliability, R, is .95, the number of redundant components needed, m, equals seven. This example illustrates the importance of high mean time to failure for individual components.

The value of redundant design depends significantly on the reliability of individual components. This is illustrated by the following example of a two-component power system.

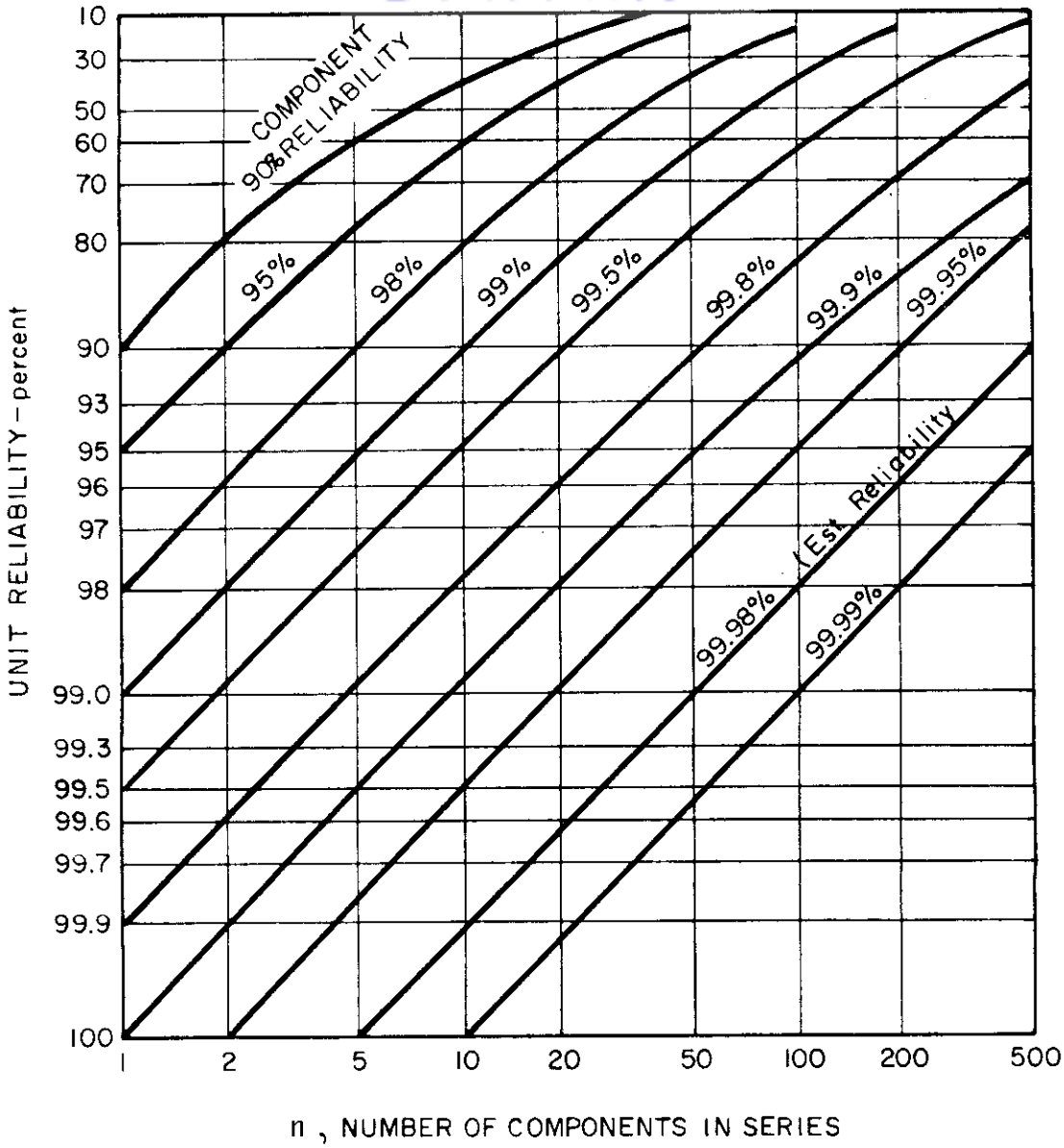

FIGURE I-C-3 UNIT RELIABILITY WITH n COMPONENTS IN SERIES

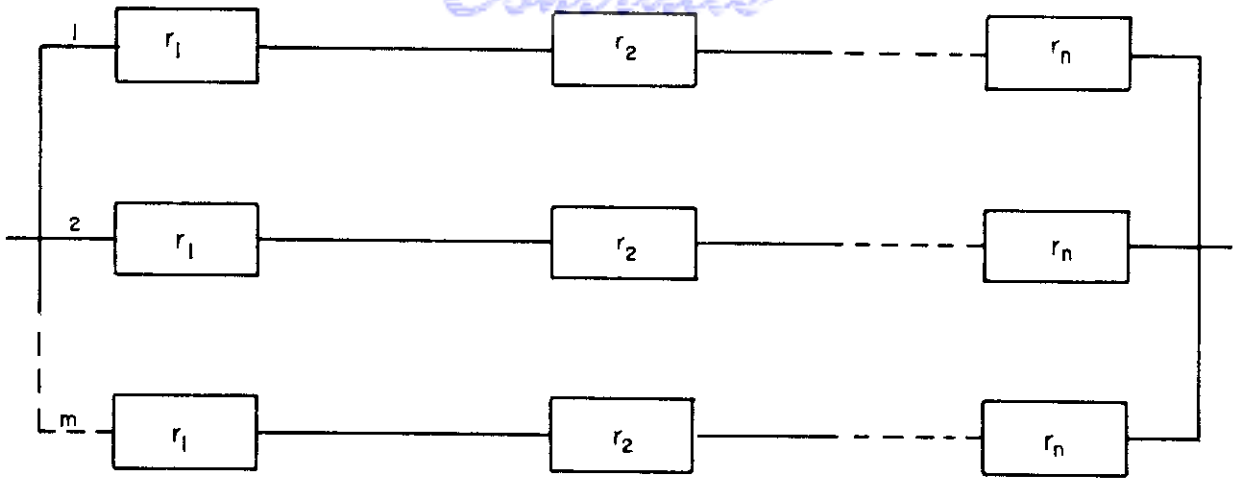

$$R = 1 - (1 - r^n)^m$$

a) PARALLEL

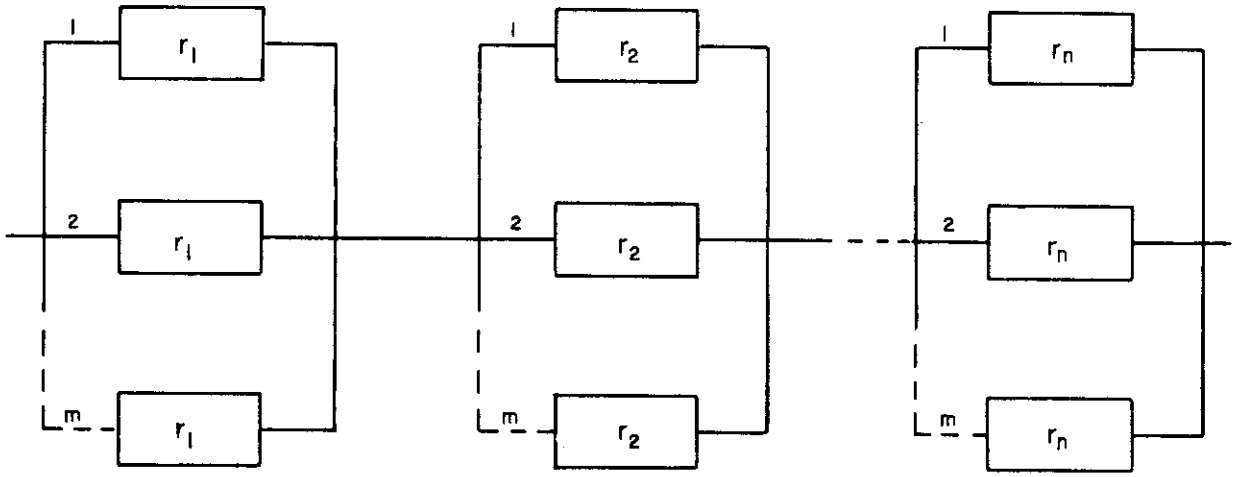

$$R = \left[1 - (1 - r)^m \right]^n$$

b) SERIES - PARALLEL

FIGURE I-C-4 REDUNDANT SYSTEMS

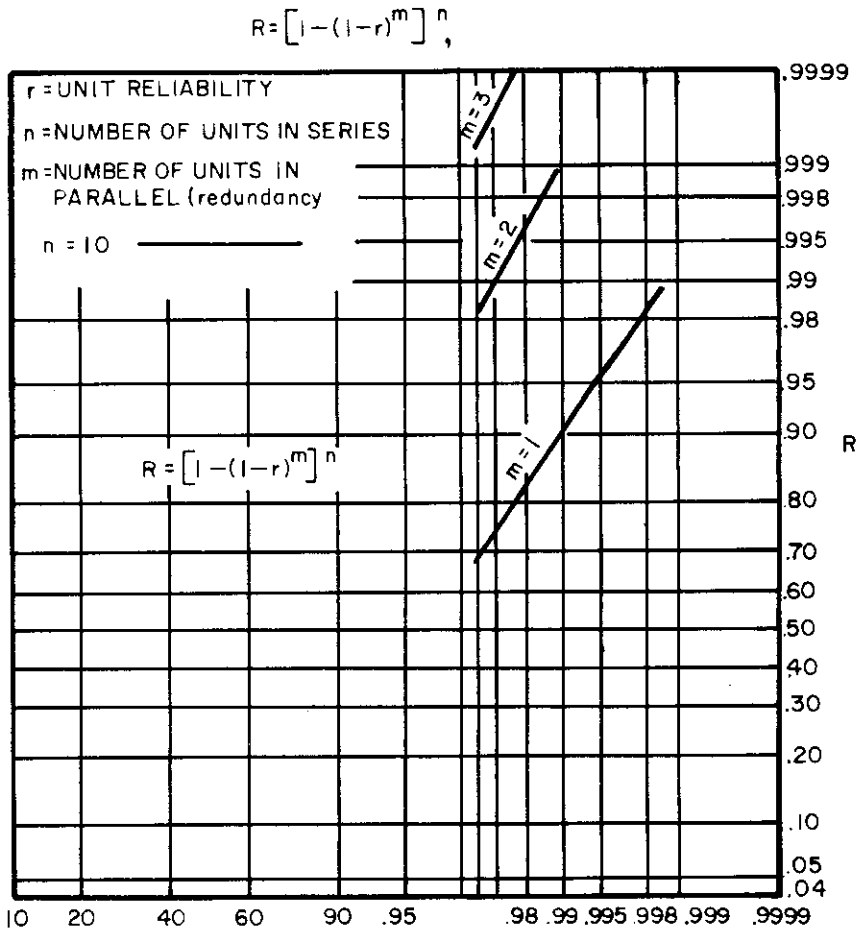

FIGURE I-C-5 OVERALL RELIABILITY AS A FUNCTION OF COMPLEXITY

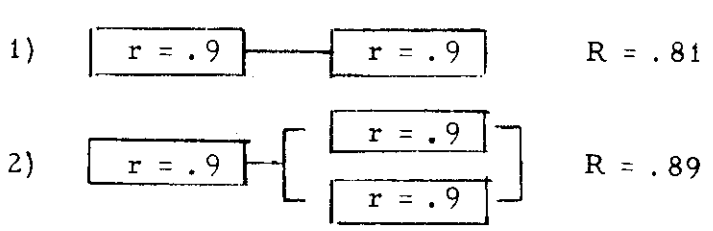

As illustrated here, redundant design is often a difficult means of achieving a significant increase in reliability.

4.0 RELIABILITY GOALS

An optimum reliability exists for any given satellite system which balances (1) the high cost of additional launchings required when low satellite reliability causes mission failure against (2) the high cost of exhaustively testing a payload (including power system) to insure high reliability. The total cost of the payload can be roughly summarized by

$$C_N = N \frac{C_L}{R_p R_L} + C_F \theta_t$$

where

C_N = total cost of achieving N successful missions

N = number of successful missions

C_L = cost of launch

R_p = reliability of payload

R_L = reliability of launch

C_F = cost of fabrication and environmental test of payload

θ_t = test time required to prove a given mean time to failure, θ_o.

An analysis of the optimum payload reliability figure is presented in Volume X, where it was assumed that $\theta_t = 2.7\,\theta_o$ from an examination of the requirements of a sequential test program. Since

$$R_p = \exp\left[-t/\theta_o\right]$$

then

$$C_N = N\frac{C_L}{R_p R_L} - \frac{C_F\,(2.7)t}{\ln R_p} \quad .$$

Therefore, the cost for a given mission can be minimized by an optimum amount of testing, which will demonstrate an optimum satellite reliability. This optimum value, R_{pm}, is given by the equation

$$\frac{R_{pm}}{(\ln R_{pm})^2} = \frac{N\,C_L}{C_F(2.7)t\,R_L}$$

and is illustrated for a specific example of a three month mission in Figure I-C-6. As shown, an extremely high value of payload reliability is not necessarily synonymous with low system cost.

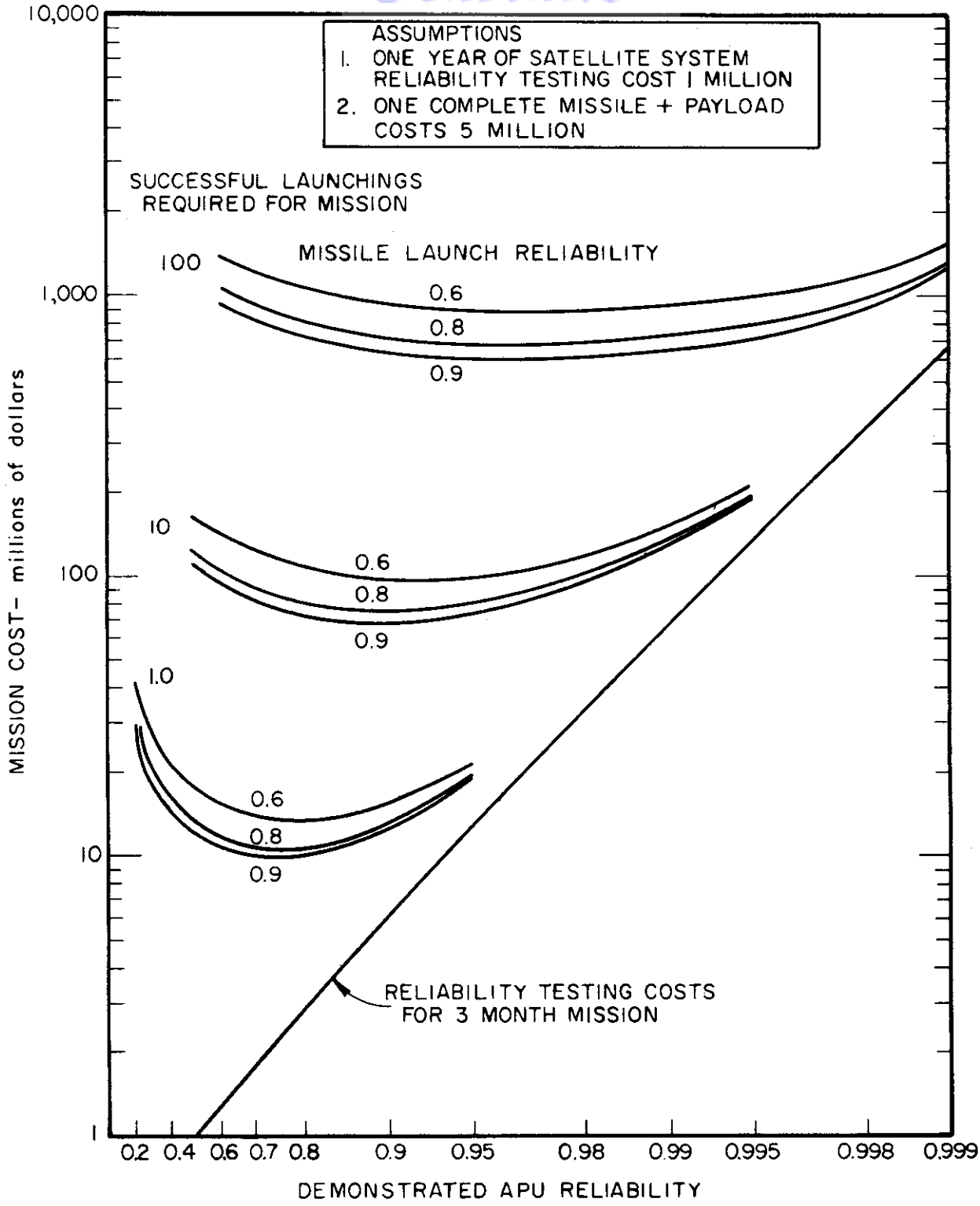

FIGURE I-C-6 OPTIMUM SATELLITE SYSTEM RELIABILITY TO MINIMIZE 3 MONTH MISSION COSTS

ENERGY CONVERSION SYSTEMS REFERENCE HANDBOOK

Volume I - General System Considerations

Section D

METHOD OF SYSTEM SELECTION AND EVALUATION

J. H. Fisher
Energy Research Division
ELECTRO-OPTICAL SYSTEMS, INC.

Manuscript released by the author
September 1960 for publication in this
Energy Conversion Systems Reference Handbook

I-D METHOD OF SYSTEM SELECTION AND EVALUATION

C O N T E N T S

I L L U S T R A T I O N

I-D METHOD OF SYSTEM SELECTION AND EVALUATION

1.0 THE PHILOSOPHY OF POWER SYSTEM EVALUATION

The quantative evaluation of advanced power systems for space utilization is presently beset with uncertainties. Many of these uncertainties will not be completely removed for many years to come. However, a quantitative evaluation is still possible provided the analyst is willing to accept a certain accuracy bandwidth or tolerance centered about the final result.

The general philosophy and structure of one particular method by which advanced power systems may be evaluated is presented below. The quantitative basis for this system evaluation technique is based on two major concepts, which rely on two sets of numerical quantities:

a. Figures of merit, and

b. Weighting factors.

When reliable numerical values can be established, then power system evaluation will become quantitative. The uncertainty associated with numerical values used in an evaluation together with the changing character of such things as cost and reliability, necessitates a generalized approach to the evaluation problem. The evaluation method adopted for this discussion relies on ratios (rather than absolute values) to establish the relative merits of different power systems.

1.1 Normalization

From a group of power systems under consideration, it is always possible to select one for which a given figure of merit can be established as best. For example, if 10 power systems are under consideration, it is possible to select one system which has the lowest estimated cost and another system (or possibly the same system) which has the highest reliability, etc. In the form described above,

figures of merit have a wide variation of absolute value and dimensionality. The normalization process establishes a numerical range of zero to unity and removes dimensionality, thus defining a "relative best" on a normalized scale.

As defined herein a normalized figure of merit is obtained by dividing the "best" value for any specific system characteristic into or by the same values obtained for all other systems under consideration. The "best" value is either numerator or denominator based on the fact that all normalized figures of merit must be less than or equal to unity.

2.0 THE TECHNOLOGY OF POWER SYSTEM EVALUATION

While many approaches to the power systems evaluation can be devised, the technique applied herein rests on two concepts -- Figures of merit and Weighting Factors.

2.1 Figures of Merit

Based on the depth to which one wishes to explore the system under consideration, the figures of merit developed can range from one or two upward to a virtually limitless variety. In evaluating power systems for space application, reasonable figures of merit might include:

a. Estimated reliability

b. Weight

c. Availability

d. Growth potential

e. Cost

f. Hazard

g. Estimated life.

In addition one might also evaluate each system in terms of regulation characteristics,

saturation properties, control requirements, and numerous other quantities. This discussion will consider only the itemized figures of merit.

2.1.1 Reliability

Meaningful reliability figures must ultimately result from actual system test experience. Nonetheless, certain basic factors are known to influence the reliability of power system hardware, including:

a. Estimated number of parts or components involved.

b. Known reliability of each part or component under suitable operating and environmental conditions.

c. Ratio of moving parts to stationary parts.

d. The redundancy and/or safety factor.

Combining these considerations, one can, to some degree, estimate the probably relative reliability of one system when compared with another. Few efforts have been made to reduce these concepts to a quantitative form. One such effort* is shown in Figure I-D-1. The originator notes that much additional effort is essential before real substance can be given to these curves. However, Figure I-D-1 represents a valid effort to make quantitative predictions concerning the relative reliability of space power systems and is offered here as an example.

*Hamilton, R. C., "Interplanetary Space Probe Auxiliary Power Systems," ARS paper No. 864-59

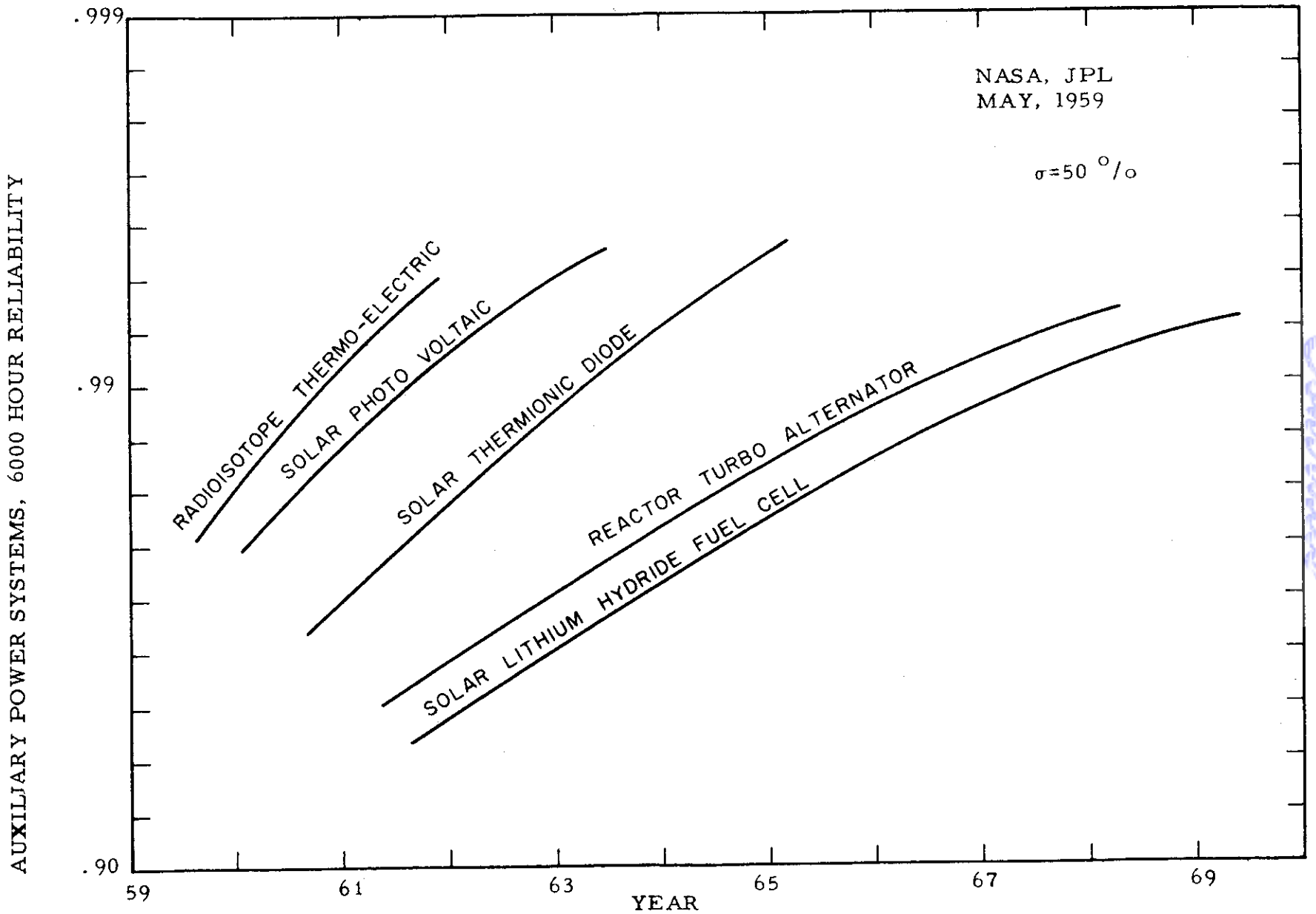

FIGURE I-D-1 ESTIMATED RELIABILITIES OF VARIOUS SPACE POWER SYSTEMS vs TIME

Let R_m be the reliability of the system estimated as the most reliable of all those being considered. Then, if R_n is the estimated reliability of the n^{th} system under consideration, its normalized figure of merit for reliability is given by:

$$F_r = \frac{R_n}{R_m}$$

2.1.2 System Weight

In a similar manner, the weight figure of merit is normalized against the lightest of the systems being considered, using reasonable component weight estimates where firm data is not available. The weight figure of merit can then be obtained using the following definition:

Y_n	=	weight per kw for component "n"
m	=	number of system components
K	=	power system capacity or rating
A	=	cumulative system efficiency compensating factor for component "n"
W_t	=	total system weight for a particular power system and
W_{tm}	=	total weight of lightest system

If the weight per kw for any component "n" is constant, the total weight of the system is given by

$$W_t = K \sum_{n=1}^{m} A_n Y_n .$$

If the weight per kw for component n varies in some other way with power, an appropriate compensating factor can be included in the above summation. The kw

rating of the n^{th} component, is given by

$$K_n = KA_n .$$

With Y_n determined, the above equation is valid and the normalized figure of merit for system weight, F_w, can be obtained from

$$F_w = \frac{W_{tm}}{K \sum_{n=1}^{m} A_n Y_n}$$

2.1.3 Availability

The availability of a particular power system to satisfy a specific need is an important but quantitatively nebulous concept. However, the quantitative evaluation of availability can be performed in a consistent, if somewhat arbitrary, fashion. For example, one can associate an availability number with a specific time or year of system availability, as illustrated:

SYSTEM OR COMPONENT AVAILABILITY

(Time Scale vs. Availability Number Entirely Arbitrary but Consistent)

Year Available	1962	1964	1966	1968	1970	1972	1974
Availability Number	10	9	8	7	6	4	2

The date of complete system availability might be based on either:

a. The projected availability date of the least developed component required for the system, or

b. The average availability of all system components.

By increasing or decreasing the amount of effort devoted to the component development, projected component availability dates can be shifted in either direction so that system availability is achieved at the earliest date.

If N_{an} is the availability number for the n^{th} component, the mean availability number for a system of "m" components is given by

$$\overline{N}_a = \frac{\sum_{n=1}^{m} N_{an}}{m}$$

If the availability number of the most advanced system is $\overline{N}_{am}$, then the normalized figure of merit for any other system is

$$F_a = \frac{\overline{N}_a}{\overline{N}_{am}}$$

2.1.4 Growth Potential

The growth potential of a system is limited by such things as:

a. Geometric and structural characteristics

b. Component power rating

c. Component efficiency

For example, thermionic diodes now available have efficiencies of 5 - 7 percent but may reach efficiencies of 15 - 30 percent with proper development. Thermal storage for these devices, however, is seriously impeded both by heat transfer

problems and by the lack of materials which retain their structural integrity at temperatures of 2,000 to 2,500°C. Thus, growth potential of diode efficiency is in theory possible but in practice depends upon the development of currently nonexistent materials for thermal storage.

Because of the constant power/area relationship for solar photovoltaic systems, their growth potential is limited by structural and geometric considerations.

Quantitative evaluation of growth potential may be even more arbitrary than that of availability. Similar tables must be developed relating component and system growth potential to numerical quantities, in which case it would be possible to obtain a normalized figure of merit of the form

$$F_g = \frac{\bar{G}_a}{\bar{G}_{am}}$$

where

$\bar{G}_a$ = the mean growth potential number for a system of m components,

$\bar{G}_{am}$ = maximum growth potential number for the best system.

2.1.5 System Cost

The normalized figure of merit for power system cost is obtained in a manner identical to that for system weight.

Using similar nomenclature, the normalized cost figure of merit is given by:

$$F_c = \frac{C_{tm}}{K \sum_{n=1}^{m} A_n X_n}$$

2.1.6 System Hazard

As an example of operational hazards, two obvious problems associated with space power systems are the presence of toxic working fluids and radioactive energy sources. Four possible conditions can be hypothesized:

a. Absence of both radioactive materials and toxic working fluids.

b. Presence of dangerous or toxic working fluid.

c. Presence of radioactivity.

d. Presence of both radioactivity and toxic working fluids.

It is possible to assign arbitrary ratings to each of these and to obtain normalized figures of merit in a. manner similar to the process employed for availability and growth potential.

2.1.7 Estimated Life

The figure of merit for estimated life can be obtained either by averaging the estimates of component life or by selecting that component with the shortest lifetime. Consideration of redundancy and the ability for self-maintenance and repair will complicate the problem.

2.2 Weighting Factor

The various figures of merit obtained for system comparison are not of equal importance. An additional factor must be included to properly weight the introduction of each figure of merit into an over-all system evaluation. The weighting factor and the normalized figures of merit are multiplied together in order to establish more nearly proper values for use in the final evaluation.

The relative importance of reliability, weight, availability, etc., is determined partly by the use for which the system is planned. For example, the presence or absence of a crew in a space vehicle may alter the importance of some hazards and also may, in fact, make the reliability of the system less critical.

Examples of possible weighting factors for manned and unmanned space operation are given below.

WEIGHTING FACTORS

	Reliability	Weight	Availability	Growth Potential	Cost	Hazard	Life
Unamnned Space Vehicle	8	7	6	5	5	3	5
Manned Space Vehicle	10	7	6	5	5	10	7

2.3 Final System Comparison

Employing normalized figures of merit and weighting factors, a total (weighted and normalized) figure of merit can be obtained for each system as follows:

Let L_i = , the i^{th} weighting factor

F_{ij} = the i^{th} normalized figure of merit for system j.

Then for p different figures of merit, the total figure of merit for the j^{th} system is:

$$S_j = \sum_{i=1}^{p} L_i F_{ij}$$

and if S_m = the maximum figure of merit found for any given system, the normalized total figure of merit for the j^{th} system is

$$(S_t)_j = \frac{\sum_{i=i}^{p} L_i F_{ij}}{S_m}$$

The quantities given by the last equation will be dimensionless and bounded between zero and unity. Providing the numerical quantities in the last equation have been obtained for one set of requirements to be applied at one specific time, a direct comparison of the quantities yields the relative over-all merit of each power system with respect to all of the others.

ENERGY CONVERSION SYSTEMS REFERENCE HANDBOOK

Volume I - General System Considerations

Section E

POWER-TIME REGIONS OF MINIMUM SYSTEM WEIGHT

W. R. Menetrey
Energy Research Division
ELECTRO-OPTICAL SYSTEMS, INC.

Manuscript released by the author
September 1960 for publication in this
Energy Conversion Systems Reference Handbook

I-E POWER-TIME REGIONS OF MINIMUM SYSTEM WEIGHT

I L L U S T R A T I O N S

I-E POWER-TIME REGIONS OF MINIMUM SYSTEM WEIGHT

Figure I-E-1 summarizes the estimates of the specific weight of solar and nuclear power systems as a function of power level. These estimates are based on component and system analyses presented in the other volumes of this handbook. As shown, several types of systems appear advantageous at different regions of power. Photovoltaic cells will continue to be used at low power levels due to their inherent simplicity and weight advantage. Solar-thermal systems appear useful in the medium power levels, while nuclear systems appear lightest at levels above roughly 20 KW. The shaded areas representing the solar systems indicate differences in weight due to different satellite altitudes and periods of darkness. Nuclear system weights can also vary significantly due to shielding requirements.

Two classes of solar systems are shown, those which could possibly be constructed by 1962-63, and estimated weights of systems possible in 1970. The nuclear systems will be developed on a time scale roughly proportional to the power level. Two systems under development are indicated, SNAP 2 (3 KW) and SNAP 8 (35 KW) with estimated flight operational dates of 1964 and 1966. Reactor thermionic systems may be developed about in the period 1968-70. Reactor thermoelectric systems will be available in the 61-63 period. 3 KW solar-mechanical systems (Rankine cycle mercury turbine, Stirling engine) may be operational in 62-63 period, while a 15 KW solar-mechanical system (Rankine cycle turbine) is under development and will be operational in the 64-65 period. Several solar-thermoelectric and solar-thermionic systems in the 100 to 1 KW range are being developed for use in 62-63, while photovoltaic systems of several hundred watt capacity will soon be used on satellite vehicles.

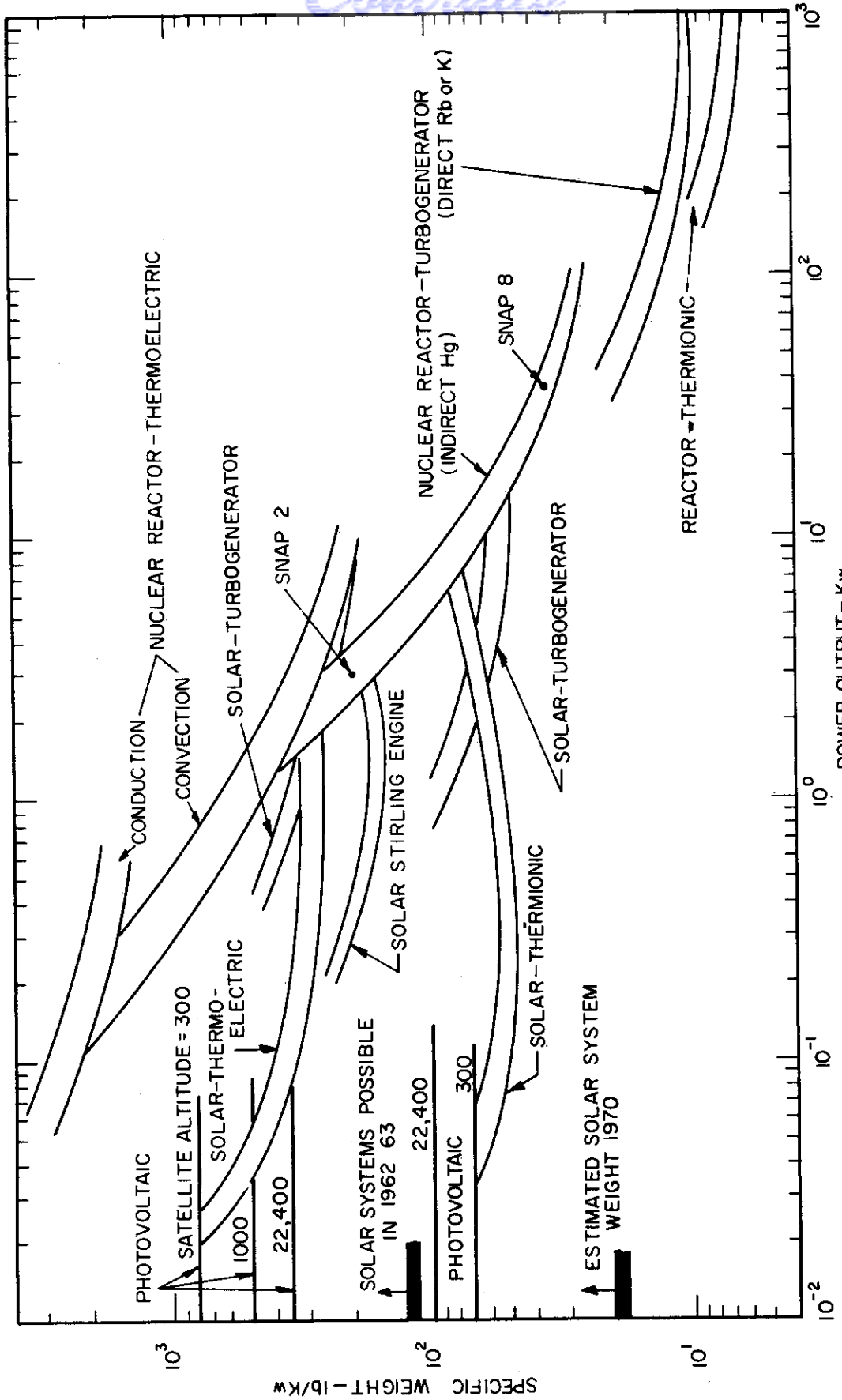

FIGURE I-E-1 ESTIMATES OF SPECIFIC WEIGHT OF SOLAR AND NUCLEAR POWER SYSTEMS

The graphs show a clear trend towards the increased use of static thermal converters at medium power levels, due primarily to the expected material improvements in these devices leading to higher efficiencies and operating temperatures.

The various types of systems may be placed in a power-time continuum, as is done in Figure I-E-2, which shows those regions where each system appears to have minimum weight compared to all others. Figure I-E-2 deals with the 1970 period, and hence is highly conjectural.

As shown, the major types of systems - chemical, solar, nuclear - are all advantageous in various regions; chemical systems for relatively short durations, solar systems for long durations up to perhaps 20 KW, and nuclear systems for long durations and high power levels.

While comparison of systems on the basis of weight is popular (perhaps because of amenability to mathematical analysis), it should be emphasized that weight alone cannot be the decisive criterion. Other factors such as reliability, cost, vehicle integration, mission integration, and other factors can play important if not leading roles in power system selection. Radioisotope power systems are a case in point: although heavier than photovoltaic systems, at power levels below one KW they offer distinct advantages in compactness and less susceptability to environmental degradation, and may be less costly. As another example, the usefulness of solar systems is a direct function of the intensity of sunlight and the amount of darkness encountered; therefore, solar power would be entirely unsuited for missions which encounter, for example, the long lunar night. Weight estimates, therefore, can only be a beginning step in selection of a power system.

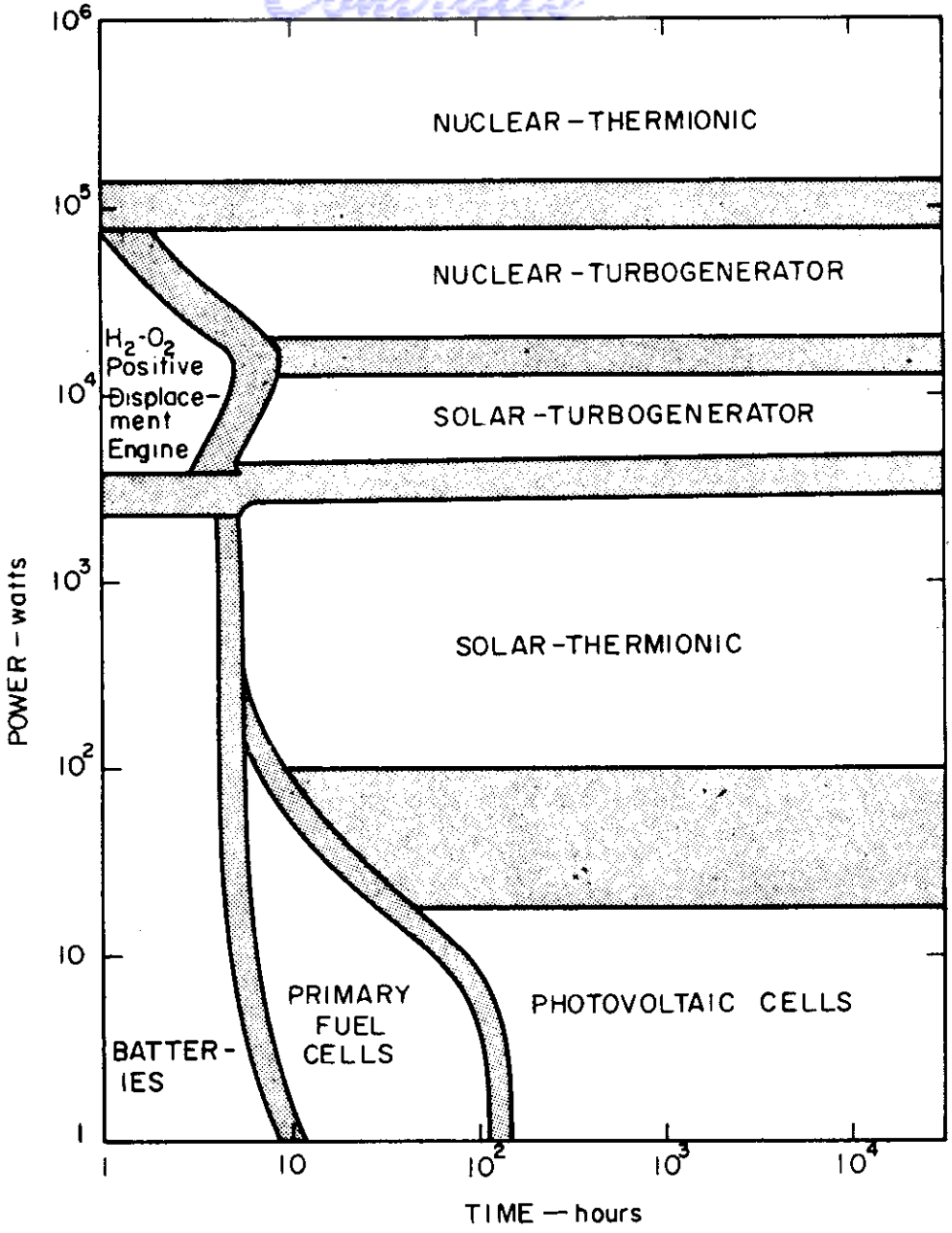

FIGURE I-E-4 ESTIMATED POWER-TIME REGIONS OF MINIMUM FOR SPACE POWER SYSTEMS--1970